ACOUSTIC WAVES GENERATED BY VORTEX SHEDDING

Thesis by

Hideki Nomoto

In Partial Fulfillment of the Requirements

for the Degree of

Aeronautical Engineer

California Institute of Technology

Pasadena, California

Submitted May 1980

ACKNOWLEDGEMENTS

I wish to express my sincere appreciation to Professor F. E. C. Culick for suggesting the problem and his constant encouragement throughout the project. Many thanks also to Professor Toshi Kubota and Dr. Kiran Magiawala for their invaluable discussions on this problem.

I am grateful to the people in GALCIT who assisted me with this research. Special thanks are due Mrs. Karen Valente for her beautiful job of typing as well as many suggestions in English.

Finally, I am indebted to the people of Mitsubishi Heavy Industries, Ltd., who gave me a chance to study abroad and supported me for two years.

ABSTRACT

An internal flow self-sustained oscillation system, which consists of a two-dimensional duct and a pair of baffles inside, is investigated experimentally. This system produces a high amplitude pure tone when certain flow and geometrical conditions are satisfied. The frequency of this generated tone seems to be determined by the longitudinal acoustic modes of the duct, while the dependence of pure tone production on flow and geometrical conditions seems to be related to the interaction between vortex shedding and acoustic feed back mechanism.

Some features on self-sustained oscillation systems are reviewed briefly and Rossiter's idea on the cavity tone system is applied for interpretation of the mechanism of the pure tone production.

Flow visualization shows stable vortical structure of the flow between the baffles when a pure tone is produced.

TABLE OF CONTENTS

TABLE OF CONTENTS (Contd.)

NOMENCLATURE

a	speed of sound
b	width of the cavity
c	average speed of sound in the cavity
d	lateral gap between the baffles = D - 2h
D	duct width
f	frequency of oscillation
f_a	longitudinal acoustic mode frequency
f_f	acoustic feedback frequency
f_i	vortex/acoustic wave interaction frequency
f_s	vortex shedding frequency
h	jet-edge distance baffle height
i	an integer
j	= 1, 2.3, 3.8, 5.4, ...
k	ratio of vortex convection velocity to reference flow velocity = U_c/U_e
ℓ	distance between baffles
L	duct length
L_1	distance from one end of the duct to the first baffle
L'	corrected duct length
ΔL	open end correction of the duct
m	an integer = $m_v + m_a$
m_a	number of acoustic waves
m_v	number of vortices
M	Mach number
n	an integer
R	Reynolds number

S	Strouhal number
t	time
U	velocity of flow
U_o	entrance velocity
U_c	vortex convection velocity
U_e	estimated reference velocity = $U_o D/d$
γ	phase difference between vortical waves and acoustic waves
γ_a	phase difference between vortical waves and acoustic waves at the upstream corner
γ_v	phase difference between vortical waves and acoustic waves at the downstream corner
λ_a	wavelength of the acoustic wave
λ_v	wavelength of the vortical wave
ν	kinematic viscosity of the fluid
φ	phase

LIST OF FIGURES

I. INTRODUCTION

Aerodynamic generation of sound has been discussed both experimentally and theoretically for a long time, but the mechanism of this phenomenon is not fully understood even for familiar musical instruments such as the flute. Studies of this sound creation by fluid flow include not only musical instruments but also undesirable phenomena in aeronautics such as airframe noise, transonic wind tunnel noise and burning instability of solid propellant rocket motors, all which are classified as self-sustained oscillating systems. (Fig. 1.1.)

One of the classical problems in sound generation by fluid motion is the edge tone phenomenon. When a wedge type structure is placed in the stream of a jet, this system produces a resonant large sound which has a dominant frequency component under certain flow and geometric conditions. The main features of the edge tone phenomenon are summarized as follows[1,2] (Fig. 1.2):

(1) For a fixed jet-edge distance, the frequency of the tone increases linearly as the velocity of the jet increases. There are minimum and maximum jet velocities beyond which no significant tone is generated. The frequency of the tone jumps to the neighboring "stage" at certain flow velocities.

(2) For a fixed jet velocity, the tone frequency decreases inversely proportional to the distance between jet exit and edge. At a certain jet-edge distance the frequency of the tone jumps to the neighboring "stage". There are minimum and maximum jet-edge distances beyond which no sound production is observed.

(3) The jumping processes in frequency in both cases exhibit hysteresis characteristics.

(4) The sound field has directional properties that are characteristic of a dipole field.

Most of these features were observed long ago, but it was only in the 1950's that this pure tone generation system was recognized and treated theoretically as one of the self-sustained oscillation systems which had an acoustic feedback mechanism coupled with a periodic hydrodynamic flow field. Because of the prominent discrete tone, theories were constructed based on the concept that the agent responsible for this sound generation was a vortex or a system of vortices shed from the corner of the jet exit. Then it was speculated that these vortices interacting with the wedge shaped structure produced pressure fluctuations which propagated upstream to stabilize the vortex shedding activities to form a closed loop feedback system. This idea of the vortex/acoustics interaction model on the edge tone system was partly supported by the flow visualization which showed vortical structure in the shear layer.

Another widely discussed example of aerodynamic sound generation is the cavity noise which also turned out to be one of the self-sustained oscillation systems. The study of flow past a cavity is complex and has several aspects of fluid mechanical problems ranging from fundamental to practical; i. e. drag and heat transfer problems, unsteady flow effects, formation of vortices in the cavity, and generation of sound. Escape hatches, open cockpits and bomb bays are practical examples of the cavity flow relating to an aircraft. The ventilation holes in transonic wind tunnel walls can also

be regarded as cavities which may contribute to noise generation.

The principal features of the sound generated by a cavity system are essentially the same as those of the edge tone system. The frequency of the emitted sound increases linearly with the flow speed for fixed cavity width, and inversely proportional to the width of the cavity for fixed flow velocity. A minimum width is required to produce sound, so is a minimum flow velocity. There are frequency jumps which form several "stages" of sound generation. A vortex or a system of vortices is observed in the cavity by the flow visualization technique.

Sound waves radiated from a cavity were clearly demonstrated by Karamcheti[3, 4], by schlieren and interferometric pictures for high speed flow. He also studied the effect of the nature of the boundary layer approaching the cavity and found that the minimum width for initially laminar flow was shorter than that for turbulent flow.

Rossiter[5], on the other hand, modelled the cavity flow with shedding vortices from the upstream corner and acoustic waves emanating from the rear corner of the cavity. He then derived a formula which described the non-dimensionalized frequency of the sound in terms of the Mach number of the flow; the ratio of vortex convection velocity to external flow velocity; and the phase difference between the vortical waves and acoustic waves at the rear corner of the cavity. This formula also includes an arbitrary integer which represents the "stage" of the radiated sound.

The generation of sound in discrete frequencies by self-sustained oscillatory systems which have strong free shear layers leads us to the structure of the shear layer. The periodic nature of

a jet was recognized a century ago as a sound sensitive jet or a singing flame and discussed by many researchers, including Lord Rayleigh[6]. A jet, once placed in an acoustic field, changes its characteristics according to the frequencies of the sound. Therefore, gas flames which used to be employed for illumination seemed to dance in harmony with the pitch of musical instruments.

In the modern study of jets, Sato[7] found sinusoidal, progressive, wave-like velocity fluctuations in the jet where the laminar flow became unstable. He also excited the jet acoustically to find that the effect of the excitation was most remarkable when the frequency of the excitation coincided with that of the intrinsic sinusoidal fluctuation. Crow and Champagne[8], on the other hand, also excited a jet acoustically and showed the large, orderly structure in jet turbulence by flow visualization.

The large, coherent structure in a mixing layer was investigated experimentally by Brown and Roshko[9]. They showed, by flow visualization, vortex-like large structures convected at nearly constant speed and amalgamating with neighboring ones to increase the sizes and spacings discontinuously.

These studies on the structure of shear layers might shed further light on the mechanism of the sound production since all the self-sustained oscillation systems have strong free shear layers and the nature of these shear flows seems to be a key factor in the study of sound generation.

The acoustic instability problem in solid propellant rocket motors is another example of the self-sustained oscillation systems. Large solid propellant rocket motors have flange-type structures

inserted between segments of the grains. These structures remain unburned while the propellant burns radially. A residual ring-shaped structure produces a strong shear flow in the chamber then constitutes a self-sustained oscillatory system with another unburned flange structure located downstream.

In the case of this internal flow, the length scales of the system include the size of the chamber as well as the distance between the unburned flanges (baffles). The latter corresponds to the distance between the jet and the wedge in the edge tone system, or to the width of the cavity in the cavity system. The chamber might play the role of a resonator which, in fact, complicates the problem.

An exploratory experimental study modelling this internal flow/acoustic interaction problem was done by Culick and Magiawala[10]. They found several acoustically excited ranges in flow speed and distance between the baffles. A simple theoretical consideration, however, gives three discrete frequency scales: the vortex shedding frequency, the acoustic feedback frequency and the frequency of the longitudinal mode of the acoustic oscillation. It was, therefore, felt that more detailed experimental work was necessary to investigate the mechanism of the sound generation in the internal self-sustained flow system.

Because of the nature of the problem which has many parameters, geometric and fluid dynamic, a new apparatus has been designed for the work reported here. The geometrical conditions such as the total length of the duct, baffle height, distance between the baffles and the location of the baffles in the duct were varied to investigate every influence of these parameters on sound production. The duct was

isolated acoustically to obtain a clear length scale for the longitudinal acoustic mode. A rectangular cross-section for the duct was chosen to get a two-dimensional flow for flow visualization. Frequencies of the generated tone were measured by a microphone while flow conditions were determined using a hot wire anemometer. Smoke flow visualization was also performed to obtain pictures of the flow between the baffles with a strobotac as a periodic light source.

In the next chapter, basic features of the self-sustained oscillation systems are reviewed in more detail while theoretical considerations particular to the internal flow systems are presented in the succeeding chapter. In Chapter 4, the experimental arrangement of the present study is described, followed by the explanation of results in Chapter 5. Discussions of the results are given in Chapter 6. Our conclusions are summarized in the final chapter.

2. SELF-SUSTAINED OSCILLATION SYSTEMS

2.1 Edge Tone System

Although the history of the study on the edge tone could be traced a century ago, G. B. Brown's experiments[11] in the 1930's were essential in the early days. He demonstrated the basic features of this phenomenon described in the previous chapter. He also derived an empirical formula for the frequency of generated sound in the following form

$$f = 0.466\ j(U-40)(\frac{1}{h} - 0.07) \qquad (2.1.1)$$

where $j = 1, 2.3, 3.8, 5.4, ---$, U is the velocity of the jet in cm/sec and h is the jet-edge distance in cm. The number j corresponds to the "stage" of the sound. He performed flow visualization at the same time which showed vortical structures of the jet flow field. But in spite of the flow visualization, his empirical formula for the frequency does not shed any light on the mechanism of the sound generation.

N. Curle[12], in 1953, proposed another formula for the frequency of the sound in a similar fashion. From an analog to the vibration of a system with damping, he assumed the relation between jet-edge distance h and wavelength λ of the vortices as follows:

$$\frac{h}{\lambda} = i + \frac{1}{4} \ , \qquad (2.1.2)$$

where i is the number of vortices in the system which also represents the stage of the sound. He then derived the convection velocity of the vortices from Brown's experimental data and finally suggested the formula for the frequency

$$f = \frac{U}{2}\left(\frac{i + \frac{1}{4}}{h} - \frac{1}{30d}\right) \quad , \tag{2.1.3}$$

where d is the width of the jet at the exit and all quantities are measured in CGS units. This extension of Brown's formula does not seem to be based on concrete support from fluid mechanics and does not include the concept of the acoustic feedback mechanism.

W. L. Nyborg's theory [13], on the other hand, is based on the idea of the displacement of the jet centerline. He derived an integral equation which determined the shape of the centerline of the jet impinging on the edge. The displacement of the centerline is expressed by the integral of the velocity of the particle which has the form

$$\eta(x, t) = \int_{t-\delta}^{t} (t - \tau) \frac{dv}{d\tau} \, d\tau \quad , \tag{2.1.4}$$

where δ is the travel time of the particle from the jet exit to the position (x, t). On the other hand, the lateral acceleration of the particle is proportional to the lateral pressure gradient. He therefore assumed that this pressure gradient could be expressed by a function of the centerline displacement at the edge multiplied by another function of the distance from the edge. Then we obtain

$$\frac{dv}{d\tau} = g[h - x] \cdot \varphi[\eta_e(\tau)] \quad , \tag{2.1.5}$$

where η_e is the displacement of the centerline at the edge. Substitution of Equation (2.1.5) into Equation (2.1.4) gives

$$\eta(x, t) = \int_{t-\delta}^{t} (t - \tau) g[h - x] \cdot \varphi[\eta_e(\tau)] \, d\tau \quad . \tag{2.1.6}$$

Particularly, at $x = h$ (at the edge), this becomes

$$\eta(h,t) \equiv \eta_e = \int_{t-\delta_o}^{t} (t-\tau)\, g[h-x]\cdot \varphi[\eta_e(\tau)]\, d\tau \quad , \qquad (2.1.7)$$

where δ_o is the total travelling time of the particle from the jet exit to the edge. This is the required integral equation which determines the unknown function η_e. Assuming some simple forms for g and φ as trial functions, Nyborg demonstrated the oscillation characters of the centerline. The integral equation formulation seems to be describing the feedback field, but the fluid dynamic, as well as acoustic, characteristics are not solved in this theory.

A. Powell[14] made an argument introducing the concept of "effectiveness" which includes an amplification rate and a phase shift of the disturbances. His idea is as follows. At first the effectiveness of the presence of the edge, η_s is derived from the interaction between the jet flow and the edge. Then the consequent fluid motion, thus resulted near the edge, gives a disturbance to the jet at the exit with effectiveness η_t. This disturbance is then communicated back to the edge with effectiveness η_d. There, the disturbance is amplified by a factor of q relative to the initial amplitude of the perturbation. With these effectiveness factors, the system is self-sustained if

$$\eta_s\, \eta_t\, \eta_d\, q = 1 \quad . \qquad (2.1.8)$$

Powell then assumed that the effect of the fluid action at the edge could be represented by a distribution of dipole sources along the edge. From this assumption he derived the expression of η_t which turned out to have a phase shift

$$\varphi_t = -\frac{\pi}{2} \quad . \tag{2.1.9}$$

This means that a disturbance originating at the edge starts a quarter cycle earlier than the disturbance arrives there.

2.2 Hole Tone System

A high tone produced by the steam action of the tea kettle is one of the familiar examples of the aerodynamic sound generation observed in our daily life. The phenomenon of the hole tone is essentially the same as that of the edge tone. The sound is classified into several sets of frequencies which are called "stages". A jumping in frequency from one stage to another occurs accompanied by hysteresis characteristics. There is a minimum distance between the exit of the jet and the hole. The frequency of the tone increases as the jet velocity increases or the jet-hole distance decreases.

Chanaud and Powell[15], using the effectiveness concept, tried to give the explanation of this phenomenon. They took into account the indirect feedback effects coming through the jet duct and surrounding outer field as well as the direct effects described in the previous section. They gave a qualitative explanation of this system but did not present any quantitative descriptions.

2.3 Choked Jet

A jet noise usually has a broad band continuous spectrum without any prominent frequency component. But when the jet pressure ratio is high enough compared to the ambient pressure, the flow in the nozzle chokes itself. Under this condition, a "whistle" or "screech" sound is observed and the overall sound pressure level is increased significantly. The discontinuity in

frequency when jet pressure is changed continuously is also observed, as are the hysteresis characteristics. This phenomenon was discussed by Powell[16, 17]. He found that the wavelength of the dominant frequency of the sound was related to the regular shock wave spacing in the flow. Hence he attributed the shock formation in the jet flow to be responsible for the feedback mechanism of the sound production system.

Hammitt[18], on the other hand, demonstrated the importance of the sound waves acting on the base regions of the jet. He then found that the jet could be stabilized significantly by shielding its base region from the sound waves.

2.4 Cavity Tone

The radiated sound waves from a cutout of a surface or of a cavity are clearly seen in schlieren and Mach-Zehnder interferometric pictures by Karamcheti[3, 4]. These pictures also show that the primary source of the acoustic waves is near the trailing edge of the cavity.

An analytical study of the mechanism of the cavity tone generation was done by Rossiter[5]. This theory is based on Powell's idea of the mechanism of choked jets. Their idea is as follows (Fig. 2.4.1). Suppose the shedding vortical waves have a wavelength λ_v. Also acoustic waves generated from the downstream corner are assumed to have wavelength λ_a. Let the width of the cavity be b. The vortices are convected with a speed of kU, where U is the uniform velocity outside of the cavity. At time $t = 0$, when an acoustic wave starts from the downstream corner, a vortex is supposed to be located at the distance $\gamma\lambda_v$ downstream of the downstream

corner. A short time later, at $t = t'$, an acoustic wave reaches the upstream corner where vortices are shed. Assume there are $m_v - 1$ vortices and m_a acoustic waves in the cavity at time $t = 0$. The frequency of these waves is expressed as

$$f = \frac{k U}{\lambda_v} = \frac{c}{\lambda_a} \quad , \tag{2.4.1}$$

where c is the mean speed of sound in the cavity. At $t = t'$, the geometric condition for the vortical waves gives

$$m_v \lambda_v = b + \gamma \lambda_v + k U t' \quad , \tag{2.4.2}$$

and for the acoustic waves

$$b = m_a \lambda_a + c t' \quad . \tag{2.4.3}$$

From these three equations we obtain a formula for the nondimensional frequency

$$\frac{f b}{U} = \frac{m_a + m_v - \gamma}{M \frac{a}{c} + \frac{1}{k}} \quad , \tag{2.4.4}$$

where $M = U/a$ is the Mach number of the outer flow. (a is the sound velocity in the outer flow.)

For a low speed case where $M = 0$, Equation (2.4.4) reduces to

$$f = \frac{U}{b} k (m - \gamma) \quad , \tag{2.4.5}$$

where

$$m = m_a + m_v \quad . \tag{2.4.6}$$

This is the formula that is compared with those of Brown (Eq. 2.1.1) or Curle (Eq. 2.1.3).

He then derived the empirical values of γ and k for shallow cavities:

$$\begin{cases} \gamma = 0.25 & (2.4.7) \\ k = 0.57 & (2.4.8) \end{cases}$$

These experimental results mean that, according to his formulation, the vortices are convected in the speed that is 57 percent of the uniform flow, and the acoustic waves begin to leave the downstream corner when a vortex is located a quarter wavelength downstream of this corner. In terms of the phase relation, this can be interpreted so that the acoustic waves have 90 degrees phase lag compared to the vortical waves at the rear corner of the cavity. This result differs from Powell's model on the edge tone system where he distributed dipole sources along the edge and brought 90 degrees advance in phase as discussed in Section 2.1. Curle's assumption on the edge tone system, which gives the relation between the jet-edge distance and wavelength, corresponds to $\gamma = -0.25$.

Bilanin and Covert[19] set up an analytical model that takes into account the stability of a vortex sheet subjected to a periodic pressure impulse. Effects of an acoustic monopole located on the downstream face of the cavity on the pressure field were also considered. After mathematical manipulation, they derived a formula for nondimensional frequency which turned out to have a similar form to that of Rossiter

$$\frac{fb}{U} = \frac{n - \frac{3}{8} - \frac{\varphi}{2\pi}}{M\frac{a}{c} - \frac{1}{k}} \qquad (2.4.9)$$

where n is an integer.

Rossiter's formula corresponds to

$$\gamma = \frac{\varphi}{2\pi} + \frac{3}{8} \quad . \qquad (2.4.10)$$

The term $\varphi/(2\pi)$ comes from the leading edge processes, while $3/8 = 0.375$ comes from the trailing edge processes which Rossiter's experiment gave a value of 0.25. Rossiter did not give the phase shift effect at the upstream corner of the cavity.

2.5 Transonic Wind Tunnel Noise

One of the causes of the noise in transonic wind tunnels which have perforated walls at the test section is considered to be produced by the edge tone mechanism. The boundary layer on the wall separates at the upstream corner of the hole forming a jet-like flow. This free shear layer, partly sucked into the plenum chamber, hits the rear corner of the hole. This free shear layer and the hole construct a self-sustained oscillation system. The hole plays the role of a cavity and sound is generated near the trailing corner of the hole.

Although the detailed mechanism is not known, some empirical suggestions have been made to prevent this undesirable, unsteady phenomenon for the wind tunnel technique. One of them relates to the proposal of the diameter of the hole. Mabey[20], from his experiment, suggested that, in order to avoid this sound radiation, the hole diameter d and the boundary layer displacement thickness δ^* along the wall should satisfy the relation

$$\frac{\delta^*}{d} < 0.5 \quad . \qquad (2.5.1)$$

He also reported that edge tones could be eliminated by reducing the tunnel wall porosity.

The edge tone in the tunnel is also reduced by covering the holes by screens[21], or inserting poles[22] or splitter plate[23] in the holes.

McCanless and Boone[24] derived an empirical formula for the nondimensional frequency of the edge tone associated with the wind tunnel in the following form:

$$\frac{f \ell_r}{U} = (j - 0.5)k(1 - 0.36\,M) \quad , \tag{2.5.2}$$

where

$$\begin{cases} k = \dfrac{U_c}{U} \quad , & (2.5.3) \\ M = \dfrac{U}{a} \quad . & (2.5.4) \end{cases}$$

ℓ_r is the longitudinal length of the hole diameter and U_c is the convection velocity of the vortex.

2.6 Jet-Edge-Resonator System

When a resonator is introduced in an edge tone system, the characteristics of the sound generation of this new system change impressively compared to the simple jet-edge system. This system has several similar features which occur in the internal flow oscillation systems. An experiment on the jet-edge-resonator system was performed by Nyborg et al[25]. They placed a tube as a resonator in a jet-edge sound field and changed the natural frequency of the tube to investigate the effect on the frequency of the generated sound. A simple edge tone system without a resonator has several stages, while each stage appears at a certain range of the jet velocity. Suppose we introduce a resonator in the sound field and change its natural frequency keeping the jet speed constant.

Frequencies of the generated sound observed in this situation change their characteristics greatly owing to the natural frequency of the resonator. In the region where the stage jump occurs for a simple jet-edge system, the frequency of the sound is determined uniquely by the natural frequency of the resonator. Even at the jet speed where only one stage of the sound is observed, other stages of the tones which are not observed regularly, can be excited by adjusting the eigenfrequency of the resonator. Sometimes subharmonics of the edge tone are included in the sound field.

2.7 Pipe Tone

A pipe with an orifice at its downstream end produces a pure tone when the flow in the pipe satisfies certain conditions. This phenomenon is known as the pipe tone or Pfeifentöne. This is another example of the oscillatory system with a resonator. As the mechanism for the excitation of this pipe tone, Anderson[26-28] argues as follows. A periodic fluctuation in the orifice area is produced by the periodic shedding of the vortices from the orifice edge. When the frequency of the pressure fluctuation caused by the vortex shedding is near one of the natural frequencies of the orifice-pipe system, the column of air in the pipe resonates to give a large level of pure tone. He also demonstrated the periodic vortex ring structure in the jet flow by flow visualization when a pure tone was produced.

2.8 Internal Flow System

One of the burning instability problems of the solid propellant rocket motors is attributed to vortex shedding in the combustion chamber coupled with acoustic oscillations. In the case of this type

of internal flow, there are three time (or frequency) scales. Culick and Magiawala[10] considered these scales as follows. The first frequency is related to the vortex shedding which is supposed to be proportional to the flow velocity U and inversely proportional to the dimension of the structure (or baffle) d from which vortices are shed. This is expressed as

$$f_s = S \cdot \frac{U}{d} \qquad (2.8.1)$$

where S is the Strouhal number. The second frequency scale is derived analogous to the theory on the edge tone mechanism. A vortex shed from the first baffle is carried downstream with the velocity of the order of U. Then an acoustic wave is generated by interaction of the vortex with the second baffle, which propagates upstream with the speed of sound. Therefore the round-trip time of these wave propagations is expressed as

$$T = \frac{\ell}{U} + \frac{\ell}{a} \quad , \qquad (2.8.2)$$

where a is the average speed of sound and ℓ is the distance between the baffles. When the flow velocity is small compared with the speed of sound, this equation gives the second characteristic frequency

$$f_f = \frac{U}{\ell} \quad . \qquad (2.8.3)$$

The third scale of the frequency is the natural longitudinal mode of the acoustic oscillation in the combustion chamber. This is given by

$$f_a = \beta \frac{a}{L} \quad , \qquad (2.8.4)$$

where L is the length scale of the chamber and β is a

proportionality factor which represents the mode of the oscillation. Assuming that the most severe resonance occurs when these three frequencies coincide, geometric and flow conditions are required to satisfy the following relations to produce pure tone:

$$\begin{cases} \frac{d}{\ell} = S & (2.8.5) \\ \frac{U}{a} = \beta \frac{\ell}{L} & (2.8.6) \end{cases}$$

Based on these considerations they performed an experiment modelling the rocket chamber flow. They used a circular cross-section pipe and two sets of orifice plates placed at several locations in the duct. In their experiment they found that acoustic modes were excited not for discrete values of flow and geometrical conditions expected from Eq. (2.8.5) and Eq. (2.8.6), but spread in distinct broad ranges of these parameters. They also found that modes having higher frequencies were excited at higher flow speed and the location of the orifice plates in the duct had a great effect on the sound production activity.

Those considerations of the acoustic waves excited in an internal flow system have motivated the work discussed here.

3. INTERNAL FLOW SYSTEMS

3.1 Definition

An internal flow system which sustains oscillations by itself consists of a duct and a pair of baffles located at an arbitrary position in the duct. Both ends of the duct are open to the surrounding field. A flow of constant mean velocity goes through the duct from one end to the other. The duct can be either axisymmetric or two-dimensional, but we consider the two-dimensional case.

3.2 Dimensional Analysis

An internal flow has the following physical variables (Fig. 3.2):

L	Duct Length,
D	Duct Width,
L_1	Distance from One End of the Duct to the First Baffle,
h	Baffle Height,
ℓ	Distance Between Baffles
U	Velocity of Flow,
a	Speed of Sound,
ν	Kinematic Viscosity of Fluid,
f	Frequency of Oscillation

There are nine variables. Since the basic dimensions for this fluid mechanical system are 3, the independent dimensionless groups are 6. They are taken as follows:

$$M = \frac{U}{a} \quad , \tag{3.2.1}$$

$$R = \frac{Uh}{\nu} \quad , \tag{3.2.2}$$

$$S = \frac{fh}{U} \quad , \tag{3.2.3}$$

$$\xi = \frac{L_1}{L} \quad , \tag{3.2.4}$$

$$\eta = \frac{h}{D} \quad , \tag{3.2.5}$$

$$\zeta = \frac{\ell}{h} \quad , \tag{3.2.6}$$

M is the Mach number of the flow and indicates the compressibility of the flow. R is the Reynolds number which is a measure of viscous effects in the fluid. S, the Strouhal number, is the nondimensionalized frequency. ξ designates the location of the baffles which might be related to the modes of the longitudinal acoustic oscillation in the duct. η is the parameter which presents the contraction ratio of the flow owing to the presence of the baffles. And finally ζ is a dimensionless measure of the depth of the cavity which is formed by the baffles and the duct wall.

3.3 Possible Frequency Scales

i) Longitudinal Acoustic Mode

An open duct of length L has longitudinal acoustic modes, of which frequencies are expressed as

$$f_a = \frac{n}{2} \cdot \frac{a}{L'} \quad , \quad (n = 1, 2, \ldots) \tag{3.3.1}$$

where

$$L' = L + \Delta L \quad . \tag{3.3.2}$$

ΔL is the open end correction and is determined by the shape of the cross-section and the conditions at the ends of the duct.

ii) Vortex Shedding

The vortex shedding frequency

$$f_s = \frac{U_c}{\lambda_v} \qquad (3.3.3)$$

is also expressed as

$$f_s = \frac{kU_e}{\lambda_v} \quad , \qquad (3.3.4)$$

where U_c is the convection velocity of the vortex, λ_v is the "wavelength" of the vortex and U_e is the reference velocity of the flow in the duct. The vortex shedding frequency can be assumed to be proportional to the flow velocity and inversely proportional to the dimension of the structure from which vortices are shed. In our case the height h of the baffle seems to be appropriate to be chosen as this length scale. Then with the Strouhal number S, we obtain

$$f_s = S \frac{U_e}{h} \quad . \qquad (3.3.5)$$

iii) Vortices/Acoustic Waves Interaction

Following Rossiter's idea, the vortical and acoustical waves are modelled as follows (Fig. 3.3.1). The vortices which are shed from the edge of the upstream baffle have a wavelength λ_v, and are convected downstream at a velocity $U_c = kU_e$. U_e is the reference velocity of the flow in the duct. At time $t = 0$, when an acoustic wave leaves the downstream baffle, there are $m_v - 1$ vortices between the baffles. The m_v^{th} vortex is located at $\gamma_v \lambda_v$ distance downstream of the second baffle. There are m_a acoustic waves between the baffles. They have a wavelength λ_a and propagate at speed c. At time $t = t'$, an acoustic wave reaches the first baffle, but a vortex cannot be generated simultaneously. This time lag can be

expressed by introducing a distance $\gamma_a \lambda_v$ which indicates the location of the imaginary vortex. The frequency of the vortical and acoustic waves are assumed to coincide at the resonance condition. Therefore

$$\frac{kU_e}{\lambda_v} = \frac{c}{\lambda_a} \equiv f_i \quad . \tag{3.3.6}$$

The geometrical condition for the vortical waves at time $t = t'$ gives

$$m_v \lambda_v = \gamma_a \lambda_v + \ell + \gamma_v \lambda_v + kU_e t' \quad , \tag{3.3.7}$$

and for the acoustic waves,

$$\ell = m_a \lambda_a + c\,t' \quad . \tag{3.3.8}$$

From Eqs. (3.3.6), (3.3.7) and (3.3.8) we obtain the equation for the frequency in nondimensional form:

$$\frac{f_i \ell}{U_e} = \frac{m_a + m_v - (\gamma_v + \gamma_a)}{M\frac{a}{c} + \frac{1}{k}} \quad , \tag{3.3.9}$$

where $M = U_e/a$ is the Mach number of the flow.

When the flow speed is low compared to the speed of sound, and for the case of the long acoustic wavelength λ_a relative to the baffle distance, in other words, if

$$\begin{cases} M \ll 1 \quad , & (3.3.10) \\ \dfrac{\lambda_a}{\ell} \gg 1 \quad , & (3.3.11) \end{cases}$$

Eq. (3.3.9) is reduced to

$$\frac{f_i \ell}{U_e} = k\{m_v - (\gamma_v + \gamma_a)\} \quad . \tag{3.3.12}$$

3.4 Resonance

A resonance is expected when the frequencies of the longitudinal acoustic mode and vortices/acoustic waves interaction coincide. Therefore putting

$$f_a = f_i \equiv f \quad , \tag{3.4.1}$$

we obtain

$$f = \frac{kU_e}{\ell} \{m_v - (\gamma_v + \gamma_a)\} \quad . \tag{3.4.2}$$

This equation is also written as

$$\frac{\ell}{U_e} = \frac{k}{f} \{m_v - (\gamma_v + \gamma_a)\} \tag{3.4.3}$$

or

$$\frac{f}{U_e} = \frac{k}{\ell} \{m_v - (\gamma_v + \gamma_a)\} \quad , \tag{3.4.5}$$

where

$$f = \frac{n}{2} \cdot \frac{a}{L'} \quad . \quad (n = 1, 2, \ldots) \tag{3.4.5}$$

4. EXPERIMENTAL ARRANGEMENT

4.1 Apparatus

Because of the nature of this problem, which has many geometric parameters, a new apparatus was designed including the application of flow visualization. The duct cross-section was chosen as a rectangular type to achieve two-dimensional flow and special care was taken for placing the baffles in the duct. The distance between the two sets of baffles are designed to be changed continuously.

The duct which has a cross-section of 5.1 cm x 15.2 cm is made of 1.27 cm thick plexiglass consisting of several sections to change the total length of the duct. Along the inner surface of the side walls two lines of grooves are cut to bury the bars which connect the baffles.

Downstream of the duct is a settling chamber, 50 cm x 50 cm x 50 cm, which is designed to reduce the turbulence level of the flow in the duct as well as to isolate the duct from other components acoustically (Fig. 4.1.1).

The flow is driven by a blower located downstream of the settling chamber. The flow speed is adjusted by the speed controller (Minarik Blue Chip II Model BCR 290). The motor is chosen as a direct current type (Minarik Blue Chip II 1.5 HP) in order to obtain fine speed adjustment. The motor has a capability to produce a flow up to 100 m/sec when a pair of baffles is installed (Fig. 4.1.2). The noise level of the blower is sufficiently low compared to the power of the resonant pure tone even at its highest speed.

A 6.4 mm thick aluminum plate is used for the baffles.

The heights of the baffles are 1.27 cm, 1.52 cm, 1.90 cm and 2.28 cm, which gives the ratios of the cross-sectional areas of the flow at the entrance of the duct to those at the baffles as 1.99, 2.48, 3.92 and 9.44, respectively. Data for the shortest baffles were not measured since no significant resonant pure tone was observed for this case. Another set of baffles of height 1.90 cm which had sharp edges (30 degrees) were also tested.

The distance between the baffles is adjusted via brass bars to which baffles are fixed by bolts. In the brass bar a long slit for the bolt was made so that the baffles can be attached at any position along the bar. These bars are buried in the grooves along the side walls in order not to disturb the flow in the duct.

The entrance and the exit of the duct are not treated aerodynamically, which leaves the open end correction problem of the longitudinal acoustic mode.

4.2 Instrumentation

A hot wire (TSI Model 1210-T1.5) was employed for the flow measurement. The wire was placed at the center of the inlet of the duct to measure the entrance velocity U_o and representative flow velocity U_e was calculated by area ratio correction:

$$U_e = \frac{D}{d} U_o$$

where D is the width of the duct and d is the gap at the baffles.

A constant temperature anemometer (GALCIT made Matilda) was used. Outputs of this anemometer were measured by a digital voltmeter (Hewlett-Packard Model 5326B).

A condenser microphone (Brüel & Kjaer Type 4134) was placed

upstream of the inlet of the duct to avoid interference. Frequencies of tone were measured by a counter (H-P Model 5326B) through an amplifier (Princeton Appl. Res. Model 189). Overall sound pressure level was measured by a true root mean square electric voltmeter (Ballantine Model 320).

Signals from the hot wire and the microphone were always monitored simultaneously by an oscilloscope (Tektronix Type 551) to check the wave form and frequency of the outputs (Fig. 4.2.1).

4.3 Flow Visualization

Flow visualization was performed by injecting kerosene vapor smoke into the flow. The flow was illuminated periodically by a strobotac (General Radio Type 1531-A) and the photographs were taken by a 35mm camera (Nikon F2A) with a 135 mm telescopic lens. Kodak Tri-X pan black and white films (ASA 400) were used.

Flow pictures were taken adjusting the frequency of the strobotac illumination so that the structures of the flow looked to be remaining at the same position.

The speed of the shutter of the camera ranged from 1/60 sec to 1/8 sec, while the aperture was kept constant (f = 2.8).

5. EXPERIMENTAL RESULTS

5.1 Description of Phenomenon

Figures 5.1.1 - 5.1.6 show the fundamental aspects of the phenomenon. These graphs are for fixed duct length (L = 50.8 cm), baffle location (L_1 = 20.0 cm) and baffle height (h = 1.90 cm). The distance ℓ between the baffles is changed from 1 cm to 6 cm. The abscissa in the estimated velocity of the flow at the baffles by the relation

$$U_e = \frac{D}{d} U_0 \quad , \qquad (5.1.1)$$

where D/d is the ratio of the cross-sectional area of the flow at the entrance of the duct to that at the baffles, and U_0 is the measured entrance velocity. The coordinate is the overall sound pressure level measured by a microphone which is placed far outside the duct entrance. The unit of the coordinate is arbitrary but is the same for Figs. 5.1.1 to 5.1.6 for comparison.

Figure 5.1.1 shows the data for baffle distance ℓ = 1.0 cm. When the flow speed goes up to 15 m/sec, the sound produced shows a significant increase in power and then decreases to the level where no pure tone is observed. The elevated sound in the neighborhood of U_e = 20 m/sec is a pure tone with clear sinusoidal wave form when monitored by an oscilloscope. When we further increase the speed of the flow, another powerful pure tone is detected near U_e = 40 m/sec and then the level of this sound decreases to the ordinary noise level with no significant frequency component.

In the case of baffle distance, ℓ = 2.0 cm, the pure tone production regions grow in numbers to three as shown in Fig. 5.1.2.

A similar behavior in sound generation activity is observed for ℓ = 3.0 cm (Fig. 5.1.3), but for ℓ = 4.0 cm, the numbers of the peaks in the sound pressure level return to two. The maximum level of the pure tone pressure varies depending on the baffle distance. In fact, the peak in sound pressure which appears at lower flow speeds shows its highest level for ℓ = 3.0 cm, while the average level does not change so much. In contrast to this first peak, the change both in level and shape of the peaks which occur at a higher flow speed is drastic as the baffle distance is varied.

For the case of sufficiently large baffle distance, ℓ = 6.0 cm, no peak in sound pressure level is observed (Fig. 5.1.6), and as a consequence no pure tone generation is achieved.

Measured pure tone frequencies for the case of ℓ = 3.0 cm are shown in Fig. 5.1.7. Pure tone is observed in three separated regions in the flow velocity, but the frequencies of sound are essentially constant throughout these regions. There is, however, a slight increase in frequency in each region when the flow speed is increased. The width of the range of the velocity where a pure tone is generated varies according to the geometrical conditions.

Another example of the measured pure tone frequencies is shown in Fig. 5.1.8. This is the case of duct length L = 92.7 cm and baffle location L_1 = 20.0 cm. Under these conditions, three modes of sound are observed in several separated regions, while in each region the frequency is nearly constant but shows a slight increase.

5.2 Longitudinal Acoustic Modes of the Duct

Longitudinal acoustic modes of the duct, with and without

baffles installed, were measured independently under no flow through the duct. A dynamic speaker was placed at the slit of the duct, and then sound was generated by a function generator. The input signal to the speaker was of a sinusoidal type and the frequency was counted by a frequency counter. A hot wire was placed in the duct to detect the fluctuations and monitored by an oscilloscope. The exciting frequency was swept in the range of interest, and from the observation of the hot wire output, the natural frequency of the duct was determined.

Prominent large oscillations of the hot wire were observed at 268 and 554 Hz for the short duct (L = 50.8 cm), and 168, 339, 511 and 674 Hz for the long duct (L = 92.7 cm). The presence of the baffles did not result in an appreciable difference in these frequencies.

With geometrical considerations, it was concluded that the longitudinal modes of the acoustic oscillation have fundamental frequencies of 268 Hz (open end correction ΔL = 12.6 cm) for the short duct and 168 Hz (ΔL = 8.5 cm) for the long duct.

5.3 Resonant Frequencies

Resonant frequency measurements were performed in various combinations of the total duct length L, the height of the baffle h and the location of the baffles in the duct L_1. (L_1 is measured from the entrance of the duct.)

i) h = 1.90 cm

Figures 5.3.1 - 5.3.4 show the case for the short duct (L = 50.8 cm). The distance ℓ between the baffles is denoted by a different symbol as indicated.

Figure 5.3.1 is the case where the baffle is located at the entrance of the duct. In general, when the flow velocity is increased, the first longitudinal acoustic mode is excited at a certain flow speed, and then it disappears and reappears again. Then the second acoustic mode is excited at a higher flow velocity. The fifth mode is excited only for ℓ = 3.0 cm and at a higher flow velocity.

Figure 5.3.2 is for the case of L_1 = 10.0 cm. At this baffle location, the activity of sound production is not strong and the second mode is not excited at all, but instead the third mode is brought about for the short baffle spacing.

Figure 5.3.3 is for L_1 = 20.0 cm. Here three regions of the second mode take place but the first mode excitation is not observed (or it is too weak to be measured with the present instrumentation). The third and the fifth modes are also excited for the case ℓ = 1.0 cm.

Figure 5.3.4 is for L_1 = 30.0 cm. The first mode reappears, but only in a narrow range of the flow velocity. Two or three regions of the second mode are observed followed by the third mode excitation at higher speeds for short baffle distance.

From Fig. 5.3.5 to Fig. 5.3.10 are the cases of the long duct (L = 92.7 cm). Figure 5.3.5 is for the baffle located at the duct entrance (L = 1.0 cm). In general the first mode is excited twice at a lower speed accompanied by one or two regions of the second mode. Higher modes are also observed for the shorter baffle spacing.

Figure 5.3.6 is for L_1 = 10.0 cm. At this baffle location, sound generation activity is not strong and regions of tone productions

are small compared to other cases.

Figure 5.3.7 is for L_1 = 20.0 cm. At this location, sound production activity is complex and several interesting features can be noticed. Consider ℓ = 2.0 cm (triangle symbols), for example. When the flow velocity goes up to 10 m/sec, the first mode appears and disappears quickly. Then the first mode reappears at about a velocity of 16 m/sec. After this mode vanishes, the third mode is excited and then disappears. Then at about 40 m/sec the fourth mode appears and disappears. Then at 48 m/sec the mode comes back to the third and disappears and then at U_e = 61 m/sec, the mode goes up to the fourth again and finally disappears.

Figure 5.3.8 is for L_1 = 30.0 cm. For this case the activity goes down again and several modes, high and low, are excited at isolated small regions of the flow velocity.

Figure 5.3.9 is for L_1 = 42.9 cm. The second mode is excited twice and the fourth mode is accompanied at a higher speed.

Figure 5.3.10 is for L_1 = 61.9 cm. The second and the third modes are excited at lower speeds while higher modes are seen at shorter baffle distance.

ii) h = 1.52 cm

Figures 5.3.11 - 5.3.14 are for lower baffle height. In general, sound production activities for the shorter height cases are less complex than those for higher height cases.

Figure 5.3.11 is for L = 50.8 cm and L_1 = 1.0 cm. Only the first mode is excited at several ranges of the velocity. In contrast, for L_1 = 20.0 cm, only the second mode is excited at two velocity ranges (Fig. 5.3.12).

Figure 5.3.13 is for the longer duct case (L = 92.7 cm) and L_1 = 1.0 cm. For this configuration three lower modes are excited at several regions while for L_1 = 20.0 cm only the third and forth modes are excited at a higher speed.

iii) h = 2.28 cm

Figures 5.3.15 and 5.3.16 are for higher baffle height and shorter duct length L = 50.2 cm. The situations for this case differ considerably compared to those of the lower baffle height. Much higher resonance frequencies are observed. Figure 5.3.15 is for the case that the baffles are placed at the entrance, and Fig. 5.3.16 is for L_1 = 20.0 cm.

This slope, or the ratio f/U_e forms the Strouhal number when a characteristic length scale is introduced. For these cases of higher baffle height, the Strouhal number seems to be fairly constant.

5.4 Non-Dimensional Frequency

The non-dimensional frequency is considered to be the slope of the line which connects the origin with the measured point in the frequency vs. velocity graphs. Since the sound frequency is almost constant in each tone production region, disregarding the baffle distance ℓ, it is appropriate to take the height of the baffle as a reference length scale. Then the non-dimensional frequency, or Strouhal number, is defined by

$$S = \frac{fh}{U_e} \quad , \qquad (5.4.1)$$

where U_e is the representative velocity of the flow, given by Eq. (5.1.1).

As the observed sound is related to the longitudinal mode of the duct, we can express the frequency of the sound as follows:

$$f = \frac{n}{2} \cdot \frac{a}{L'} \quad , \quad (n = 1, 2, \ldots) \tag{5.4.2}$$

where a is the velocity of the sound, n is an integer which represents the mode and L' is the length scale of the duct which differs slightly from the actual geometric length because of the open-end correction. (Here we assumed an open pipe configuration.) Substitution of Eq. (5.4.2) into Eq. (5.4.1) gives

$$S = \frac{n}{2} \cdot \frac{a}{L'} \cdot \frac{h}{U_e} \quad . \tag{5.4.3}$$

When we introduce the Mach number by

$$M = \frac{U_e}{a} \quad , \tag{5.4.4}$$

Eq. (5.4.3) is expressed as

$$S = \frac{n}{2} \cdot \frac{h}{L'} \cdot \frac{1}{M} \quad . \tag{5.4.5}$$

Therefore, for fixed geometrical conditions, the Strouhal number is inversely proportional to the Mach number, and the number which indicates the mode is included in the proportionality constant.

Some examples for this Strouhal number vs. Mach number plotting are shown in Figs. 5.4.1 - 5.4.10. As can be expected from the frequency data in terms of velocities, the Strouhal numbers for the generated sound lie in certain regions, though there seems to be some dependence on the height of the baffles. In general,

Strouhal numbers are in the range:

$$\begin{cases} 0.1 \leq S \leq 0.6 \ , & (h = 1.90 \text{ cm}) \quad (5.4.6) \\ 0.1 \leq S \leq 0.3 \ , & (h = 1.52 \text{ cm}) \quad (5.4.7) \\ 0.5 \leq S \leq 1.0 \ . & (h = 2.28 \text{ cm}) \quad (5.4.8) \end{cases}$$

5.5 Pure Tone Production Regions

Pure tone production regions are shown in terms of flow velocity and distance between baffles in Figs. 5.5.1 - 5.5.16. Numbers denoted at each region indicate the mode of the generated sound. Narrow regions are shown as lines and isolated points, instead of regions, are also included as circles or horizontal lines. In general, higher modes are observed at a higher speed and the tone production region shifts to the higher speed side when the distance between the baffles is increased.

i) h = 1.90 cm

Figures 5.5.1 - 5.5.4 are cases for the short duct. The first mode is about 270 Hz, the second mode 540 Hz, and so on. In general the first mode appears at low speed and the higher modes (up to the third) appear at a higher speed. There seems to be a minimum speed to produce pure tone.

Figures 5.5.5 - 5.5.10 are for the long duct. The frequency of the first mode is about 160 Hz and the second mode 320 Hz, and so on. General characteristics -- modes are lower at low speed and higher at high speed -- can also be seen for these cases. It is clear that a minimum speed is required to produce a pure tone, but the requirement for the minimum distance is not clear.

ii) h = 1.52 cm

The situation is less complex for this baffle height. The shorter baffle regions where pure tone is produced are clearly separated from each other. Only one mode is observed in each case for the short duct (Figs. 5.5.11-12), while several modes are detected for the long duct (Figs. 5.5.13-14).

iii) h = 2.28 cm

As was expected from the frequency graphs, the regions of the sound production are scattered, consisting of many small islands. Higher modes are, in general, excited at a higher flow velocity (Figs. 5.5.15-16).

5.6 Velocity Field Between the Baffles

i) Centerline Velocity

Because of the complex flow field in the duct near the baffles, the correct velocity at the baffle cannot be estimated by a simple geometric condition expressed by Eq. (5.1.1).

The actual velocity measurement was done by placing a hot wire between the baffles on the duct centerline. The results are shown for the two cases of baffle height. Figure 5.6.1 is for $h = 1.90$ cm or $D/d = 3.92$, where D and d are cross-sectional areas at the entrance of the duct and that at the baffle, respectively. The centerline velocity, in general, exceeds the value of D/d for the shorter baffle spacing or for lower flow velocity, while for the larger baffle spacing it seems to be a good first approximation.

Figure 5.6.2 is for $h = 1.52$ cm ($D/d = 2.48$). For this shorter baffle case, the centerline velocity seems to be independent

of the baffle distance and indicates slightly higher values than D/d. But U_e given by Eq. (5.1.1) seems to be a good first approximation.

ii) Velocity Profile

The velocity profile between the baffles was measured by traversing the hot wire probe across the duct. An example for h = 1.9 cm is shown in Fig. 5.6.3. As is clearly shown from this figure, a strong jet-like shear profile is achieved between the baffles.

The velocity on the line which connects the edges of the baffles seems to be about 50 percent of the center velocity.

5.7 Flow Visualization

Flow visualization was performed for the long duct (L = 92.7 cm) with baffles of height h = 1.90 cm located at the entrance of the duct (L_1 = 1.0 cm). Both blunt and sharp edge baffles are employed for this purpose, but no essential difference was detected between them.

For each configuration the flow speed was adjusted so that the acoustic resonance was obtained at the lowest flow velocity, but it was also tried for higher speed. Under these resonant conditions a very stable vortex or vortices were observed by adjusting the frequency of the strobotac illumination. Out of the region of pure tone production stable vortices are difficult to obtain except for very slow speeds where regular vortical shedding activity is observed.

Figures 5.7.1 and 5.7.2 are for the baffle spacing ℓ = 1.0 cm. At flow velocity U_e = 14 m/sec (Fig. 5.7.1), a vortex is formed between the baffles, while at a higher speed U_e = 23 m/sec (Fig.

5.7.2), two vortices, though smaller in scale, are seen along each side of the flow.

Figures 5.7.3 and 5.7.4 are for the baffle spacing ℓ = 3.0 cm. These pictures also show the increase in number of vortices between the baffles when the resonance is obtained at a higher flow speed.

The vortices observed under these resonant conditions are symmetric along the centerline of the duct.

6. DISCUSSION

6.1 Mechanism of Sound Production

As can be seen from the comparison of the pure tone frequency with the longitudinal acoustic modes of the duct (Figs. 5.3.1 - 5.3.16), the frequency of the generated tone is directly related to the natural frequency of the duct. The appearance and disappearance of the pure tone production activity, however, seems to be related to the interaction of vortices shed from the first baffle with the acoustic waves generated at the second baffle. In other words, in the figure of frequency f vs. velocity U_e (Fig. 6.1.1), the horizontal line

$$f = f_i \quad (i = 1, 2, \ldots) \tag{6.1.1}$$

is determined by the longitudinal mode of the duct. Here f_i's are the natural frequency of the duct. The slope f/U_e, on the other hand, is determined by the interactions between the vortex shedding and acoustic waves, which is given by Eq. (3.4.5):

$$\frac{f}{U_e} = \frac{k}{\ell} \{m_v - (\gamma_v + \gamma_a)\} \quad (m_v = 1, 2, \ldots) \tag{6.1.2}$$

The integer m_v brings in the discrete feature of the tone production. The intersections of the lines expressed by Eq. (6.1.1) and the lines represented by Eq. (6.1.2) are the points where pure tone production can be achieved.

An example of the application of this idea to the actual data is shown in Fig. 6.1.2 for $L = 92.7$ cm, $h = 1.90$ cm, $L_1 = 20.0$ cm and $\ell = 3.0$ cm.

6.2 Pure Tone Production Regions

Under fixed geometrical conditions ($\ell = \ell_1$), points of pure tone

production are the intersections of the graphs expressed in the following equations:

$$\begin{cases} \dfrac{f}{U_e} = \dfrac{k}{\ell_1} \{m_v - (\gamma_v + \gamma_a)\} \quad (m_v = 1, 2, \ldots) & (6.2.1) \\ f = f_i \quad (i = 1, 2, \ldots) & (6.2.2) \end{cases}$$

Suppose these points are designated, in the $f - U_e$ plane, as A for $m_v = 1$, $i = 1$, B for $m_v = 2$, $i = 1$, C for $m_v = 3$, $i = 1$, D for $m_v = 1$, $i = 2$, E for $m_v = 2$, $i = 2$ and F for $m_v = 3$, $i = 2$ as shown in Fig. 6.2.1(a). We assume k is constant. When we change the baffle distance ℓ from ℓ_1 to ℓ_2, point A moves to point A' in the $\ell - U_e$ plane (Fig. 6.2.1(b)) on the line which is described by the equation

$$\frac{\ell}{U_e} = \frac{k}{f_1} \{1 - (\gamma_v + \gamma_a)\} \quad . \qquad (6.2.3)$$

Similarly, points B and C move to B' and C' satisfying

$$\frac{\ell}{U_e} = \frac{k}{f_1} \{m_v - (\gamma_v + \gamma_a)\} \quad , \qquad (6.2.3)$$

and $m_v = 2$ and 3 for B and C, respectively. In the $f - U_e$ plane (Fig. 6.2.1(a)), point A moves to A' horizontally, since the frequency is determined by the longitudinal acoustic mode. Similarly B and C move on the line of $f = f_1$ and D, E and F move on the line of $f = f_2$ to each primed point.

Assume there are maximum and minimum Strouhal numbers beyond which no vortex shedding can be attained. (The fact that the Strouhal number for vortex shedding is restricted in the range of 0.1 to 0.5 for outer flow cases seems to support this assumption.) These maximum and minimum values give lines of

$$\begin{cases} \dfrac{f}{U_e} = S_{max}/h & (6.2.4) \\ \dfrac{f}{U_e} = S_{min}/h & (6.2.5) \end{cases}$$

in the $f - U_e$ plane. Therefore, tone production is only achieved in the regions

$$S_{min}/h \leq \frac{f}{U_e} \leq S_{max}/h \quad , \qquad (6.2.6)$$

and on the lines expressed by Eq. (6.2.2). Then the restriction (6.2.6) is transformed in terms of the velocity to give

$$U_{e_{i,min}} \leq U_e \leq U_{e_{i,max}} \quad , \ (i = 1, 2, \ldots) \qquad (6.2.7)$$

where i corresponds to each acoustic mode.

Coming back to the $\ell - U_e$ plane, Eq. (6.2.6) sets the interval in U_e for each mode where tone production is actually achieved. These intervals confine the sound production activity, eliminating points such as C, F, A' and D'. The final tone production regions are defined by the heavy lines in Fig. 6.2.1(b).

The intersection of

$$\begin{cases} f = f_1 & (6.2.8) \\ f/U_e = h \cdot S_{max} & (6.2.9) \end{cases}$$

in the $f - U_e$ plane gives the minimum velocity for pure tone production. The intersections of

$$\begin{cases} U_e = U_{e_{i,min}} & (6.2.10) \\ \ell/U_e = \dfrac{k}{f_i} \{1 - (\gamma_v + \gamma_a)\} & (6.2.11) \end{cases}$$

in the $\ell - U_e$ plane give the minimum baffle distance ℓ_{min} for tone production.

The discussions so far are based on the assumption that k, the vortex convection coefficient, is constant regardless of the flow velocity or the baffle distance. But k is a function of all non-dimensionalized parameters derived in Section 3.2, and, in fact, it is believed to be a strong function of $R = Uh/\nu$, $\eta = h/D$ and $\zeta = \ell/h$. Taking these parameters into account causes distortions in the graphs of vortices/acoustic waves interaction frequency, instead of straight lines. But the essential feature that pure tone is produced at the intersection described by Eqs. (6.2.1) and (6.2.2) remains appropriate. Here.

$$k = k(D,\ U,\ h,\ \ell) \quad . \tag{6.2.12}$$

6.3 Other Aspects of the Experimental Results

The actual experimental results show the width of the tone production region in the ℓ - U_e plane. This fact is supposed to be due to the damping effect of the oscillation system. The slight increase in frequency in each region can be attributed to the change of the end effect of the duct due to the change of the mean flow velocity, or to strong vortex shedding which distorts the resonance frequency of the system.

6.4 Application of the Formula to the Present Data

According to the model of pure tone production mechanism discussed so far, the pure tone is obtained on the line of

$$\frac{\ell}{U_e} = \frac{k}{f_i}(m - \gamma) \quad , \quad (m = 1, 2, \ldots) \tag{6.4.1}$$

where

$$\begin{cases} m = m_v \ , & (6.4.2) \\ \gamma = \gamma_v + \gamma_a \ . & (6.4.3) \end{cases}$$

Present experimental data gives the values of ℓ, U_e and f_i. Therefore, Eq. (6.4.1) is considered to be an equation which determines the unknown variables k and γ. (m is easily assumed.) In approximating the experimental data by the equations $\ell/U_e = c_1$ and c_2, $f_i = f$, $m = m_1$ and m_2, we have a system of simultaneous equations for k and γ:

$$\begin{cases} \frac{k}{f}(m_1 - \gamma) = c_1 & (6.4.4) \\ \frac{k}{f}(m_2 - \gamma) = c_2 \ . & (6.4.5) \end{cases}$$

The solution of this system is given by

$$\begin{cases} \gamma = \frac{c_1 m_1 - c_2 m_1}{c_1 - c_2} & (6.4.6) \\ k = \frac{c_1 - c_2}{m_1 - m_2} f \ . & (6.4.7) \end{cases}$$

From the data for $L = 92.7$ cm, $L_1 = 20.0$ cm, $h = 1.90$ cm and $\ell = 3.0$ cm, these values are calculated for several combinations of modes and vortex numbers. The mean values of this calculation are

$$\begin{cases} \gamma = -0.476 & (6.4.8) \\ k = 0.148 \ . & (6.4.9) \end{cases}$$

This result in phase γ is in good agreement with Sarohia's data[29,30] on cavity tone which gives the value

$$\gamma = -0.5 \ . \qquad (6.4.10)$$

On the other hand, both Curle's assumption on jet-edge distance and wavelength relation and Powell's formulation on the edge tone system give

$$\gamma = -0.25 \quad , \tag{6.4.11}$$

showing appreciable differences from our data.

Calculations for other configurations are summarized in Table 6.4.1 and show scatter of the data in the range

$$\begin{cases} -0.7 \leq \gamma \leq 0 & (6.4.12) \\ 0.1 \leq k \leq 0.4 \quad . & (6.4.13) \end{cases}$$

7. CONCLUDING REMARKS

An internal flow self-sustained oscillation system has been investigated experimentally and the following conclusions have been obtained.

(1) An internal flow system with a pair of baffles inside is a self-sustained oscillation system in which the longitudinal acoustic mode locks in with the vortex shedding from the baffle to produce a high amplitude pure tone.

(2) Rossiter's model for the cavity tone system is applied for an interpretation of the mechanism of pure tone production of the internal flow system.

(3) According to the height of the baffles, the system may be classified into three cases: (i) Low baffles produce lower longitudinal modes of sound over relatively broad ranges of conditions (Fig.5.5.12); (ii) High baffles produce higher modes of longitudinal oscillations at isolated flow and geometrical configurations (Fig.5.5.16); and (iii) Middle height baffles produce complex combinations of modes and tone production regions (Fig.5.5.7).

(4) There seems to be a minimum velocity for the production of a pure tone, but the existence of a minimum spacing of the baffles is not clear from the present experiments. The existence of a minimum velocity and minimum spacing can be predicted theoretically if we assume that the vortex shedding frequency is restricted to certain ranges of the Strouhal number.

(5) Flow visualization shows stable vortical structure in

the flow between the baffles when a pure tone is produced.

(6) Application of Rossiter's formula to the present data fails to determine the phase difference between vortical and acoustic waves. That sort of model is inappropriate to interpret the phenomenon in detail.

REFERENCES

1. Karamcheti, K., Bauer, A.B., Shields, W.L., Stegen, G.R. and Wooley, J.P. "Some Features of an Edgetone Flow Field", Basic Aerodynamic Noise Research, NASA SP-207 (1969) pp. 275-304.

2. Holger, D.K., Wilson, T.A. and Beavers, G.S. "Fluid Mechanics of the Edgetone", J. Acoust. Soc. Am., Vol. 62, No. 5 (1977) pp. 1116-1128.

3. Karamcheti, K. "Acoustic Radiation from Two-Dimensional Rectangular Cutouts in Aerodynamic Surfaces", NACA TN-3487, (1955).

4. Karamcheti, K. "Sound Radiation from Surface Cutouts in High Speed Flow", Ph.D. Thesis, California Institute of Technology, (1956).

5. Rossiter, J.E. "Wind Tunnel Experiments on the Flow Over Rectangular Cavities at Subsonic and Transonic Speeds", ARC RM 3438 (1964).

6. Rayleigh, J.W.S. The Theory of Sound, Dover (1945).

7. Sato, H. "The Stability and Transition of a Two-Dimensional Jet", J. Fluid Mech., Vol. 7 (1960) pp. 53-80.

8. Crow, S.C. and Champagne, F.H. "Orderly Structure in Jet Turbulence", J. Fluid Mech., Vol. 48, No. 3 (1971) pp. 547-591.

9. Brown, G.L. and Roshko, A. "On Density Effects and Large Structure in Turbulent Mixing Layers", J. Fluid Mech., Vol. 64, No. 4 (1974) pp. 775-816.

10. Culick, F.E.C. and Magiawala, K. "Excitation of Acoustic Modes in a Chamber by Vortex Shedding", J. Sound and Vib., Vol. 64, No. 3 (1979) pp. 455-457.

11. Brown, G.B. "The Vortex Motion Causing Edge Tones", Proc. Phys. Soc. (London), Vol. 49 (1937) pp. 493-509.

12. Curle, N. "Mechanics of Edge-Tones", Proc. Roy. Soc., Vol. A 216 (1953) pp. 412-424.

13. Nyborg, W.L. "Self-Maintained Oscillations of the Jet in a Jet-Edge System. Part I", J. Acoust. Soc. Am., Vol. 26, No. 2 (1954) pp. 174-182.

14. Powell, A. "On the Edgetone", J. Acoust. Soc. Am., Vol. 33, No. 4 (1961) pp. 395-409.

15. Chanaud, R.C. and Powell, A. "Some Experiments Concerning the Hole and Ring Tones", J. Acoust. Soc. Am., Vol. 37, No. 5 (1965) pp. 902-911.

16. Powell, A. "On the Noise Emanating from a Two-Dimensional Jet Above the Critical Pressure", Aeronautical Quarterly, Vol. 4 (1953) pp. 103-122.

17. Powell, A. "On the Mechanism of Choked Jet Noise", Proc. Phys. Soc., Ser. B, Vol. 66 (1953) pp. 1039-1056.

18. Hammitt, A.G. "The Oscillation and Noise of an Overpressure Sonic Jet", J. Aerospace Sci., Vol. 28, No. 9 (1961) pp. 673-680.

19. Bilanin, A.J. and Covert, E.E. "Estimation of Possible Excitation Frequencies for Shallow Rectangular Cavities", AIAA Journal, Vol. 11, No. 3 (1973) pp. 349-351.

20. Mabey, D.G. "Flow Unsteadiness and Model Vibration in Wind Tunnels at Subsonic and Transonic Speeds", ARC CP 1155 (1970).

21. Schutzenhofer, L.A. and Howard, P.W. "Suppression of Background Noise in a Transonic Wind-Tunnel Test Section", AIAA Journal, Vol. 13, No. 11 (1975) pp. 1467-1471.

22. Dougherty, N.S., Jr., Anderson, C.F. and Parker, R.L. "An Experimental Investigation of Techniques to Suppress Edgetones from Perforated Wind Tunnel Walls", AEDC-TR-75-88 (1975).

23. Jacobs, J.L. "Aerodynamic Characteristics of Perforated Walls for Transonic Wind Tunnels", AEDC-TR-77-61 (1977).

24. McCanless, G.F., Jr. and Boone, J.R. "Noise Reduction in Transonic Wind Tunnels", J. Acoust. Soc. Am., Vol. 56, No. 5 (1974) pp. 1501-1510.

25. Nyborg, W.L., Burkhard, M.D. and Schilling, H.K. "Acoustical Characterstics of Jet-Edge and Jet-Edge-Resonator Systems", J. Acoust. Soc. Am., Vol. 24, No. 3 (1952) pp. 293-304.

26. Anderson, A.B.C. "Dependence of Pfeifenton (Pipe Tone) Frequency on Pipe Length, Orifice Diameter, and Gas Discharge Pressure", J. Acoust. Soc. Am., Vol. 24, No. 6 (1952) pp. 675-681.

27. Anderson, A.B.C. "A Circular-Orifice Number Describing Dependence of Primary Pfeifenton Frequency on Differential Pressure, Gas Density, and Orifice Geometry", J. Acoust. Soc. Am., Vol. 25, No. 4 (1953) pp. 626-631.

28. Anderson, A. B. C. "Structure and Velocity of the Periodic Vortex-Ring Flow Pattern of a Primary Pfeifenton (Pipe Tone) Jet", J. Acoust. Soc. Am., Vol. 27, No. 6 (1955) pp. 1048-1053.

29. Sarohia, V. "Experimental and Analytical Investigation of Oscillations in Flow Over Cavities", Ph.D. Thesis, California Institute of Technology (1975).

30. Sarohia, V. "Experimental Investigation of Oscillations in Flows Over Shallow Cavities", AIAA Paper 76-182 also: AIAA Journal, Vol. 15, No. 7 (1977) pp. 984-991.

Table 6.4.1

Application of Rossiter's Formula to the Present Data

L (cm)	L_1 (cm)	h (cm)	Mode	γ	k
50.8	1.0	1.90	1	-0.425	0.197
50.8	1.0	1.90	2	-0.684	0.167
50.8	20.0	1.90	2	-0.286	0.203
				-0.407	0.186
				-0.762	0.168
92.7	1.0	1.90	1	-0.093	0.120
92.7	1.0	1.90	2	-0.584	0.111
92.7	20.0	1.90	3	-0.475	0.148
				-0.460	0.149
				-0.466	0.148
92.7	20.0	1.90	4	-0.755	0.131
				-0.175	0.166
				-0.546	0.149
50.8	1.0	1.52	1	-0.185	0.184
				-0.145	0.381
				-0.041	0.197
50.8	20.0	1.52	2	-0.237	0.188

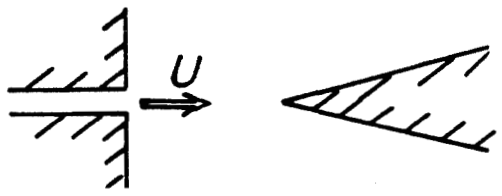

a) Edge Tone System.

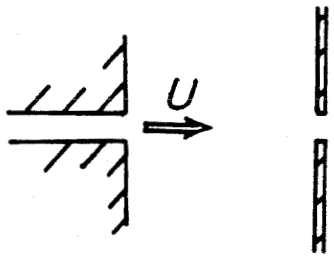

b) Hole Tone System.

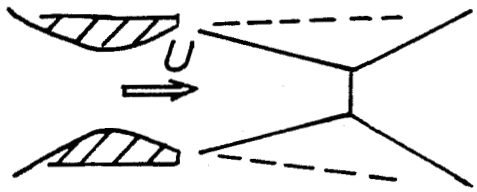

c) Choked Jet.

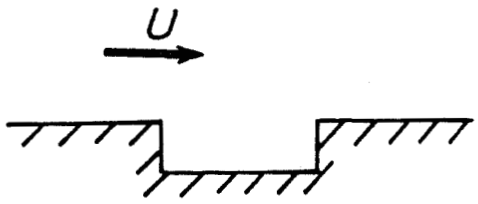

d) Cavity Tone System.

Fig.1.1. Self-Sustained Oscillation Systems.

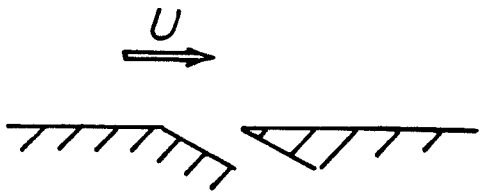

e) Perforated Transonic Wind Tunnel Wall.

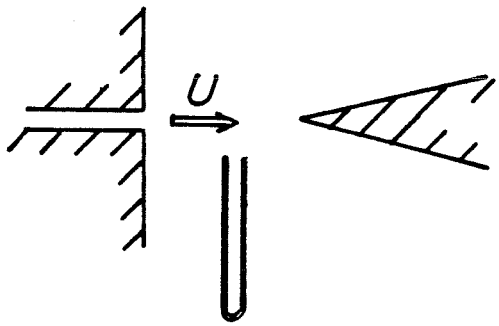

f) Jet-Edge-Resonator System.

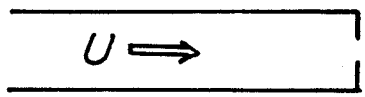

g) Pipe Tone System.

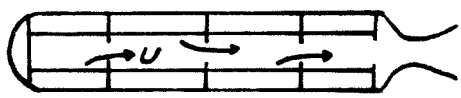

h) Solid Propellant Rocket Motor.

Fig.1.1. (Concluded)

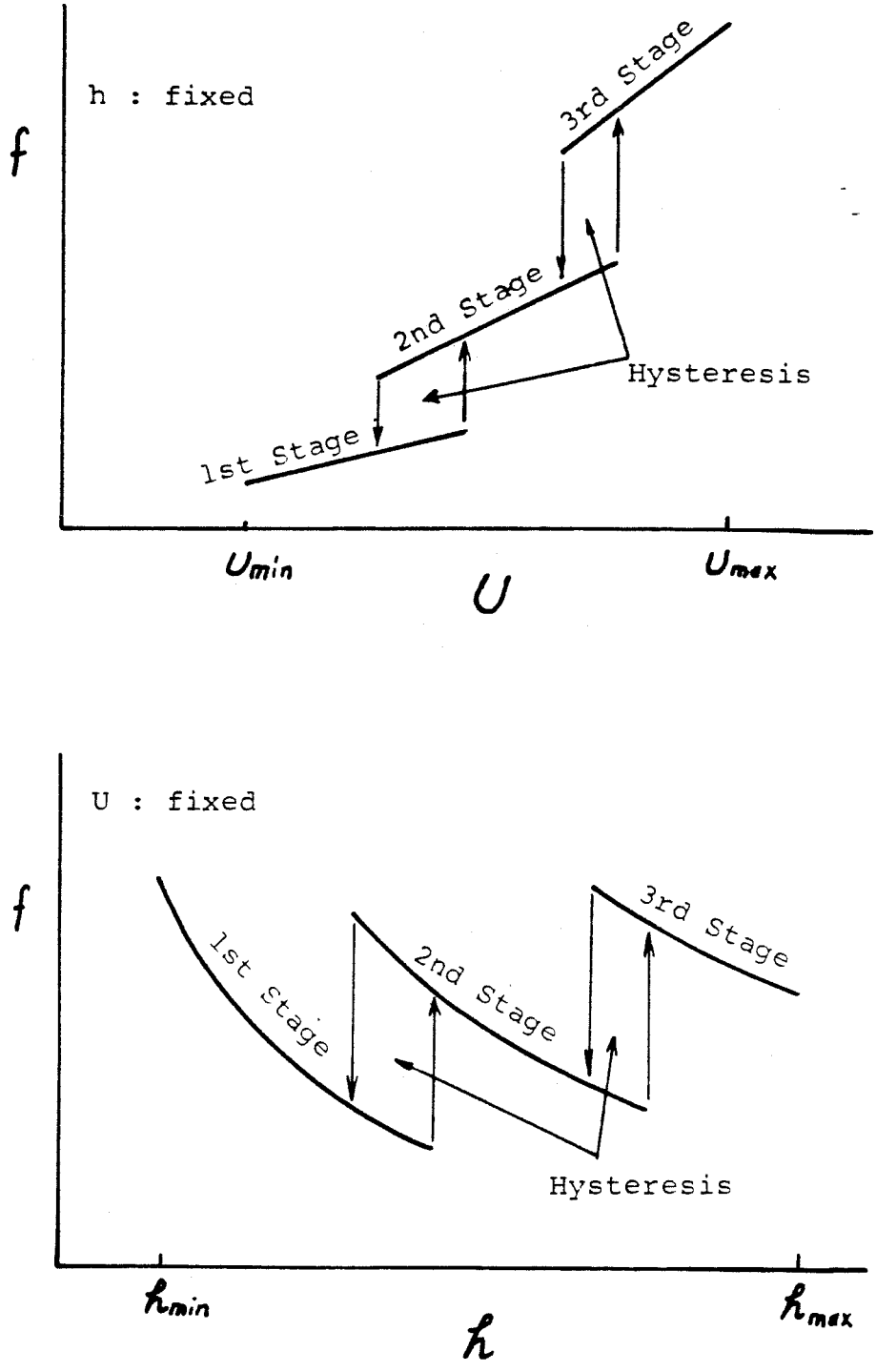

Fig.1.2. Dependence of Edge Tone Frequency on Jet Velocity U and Jet-Edge Distance h.

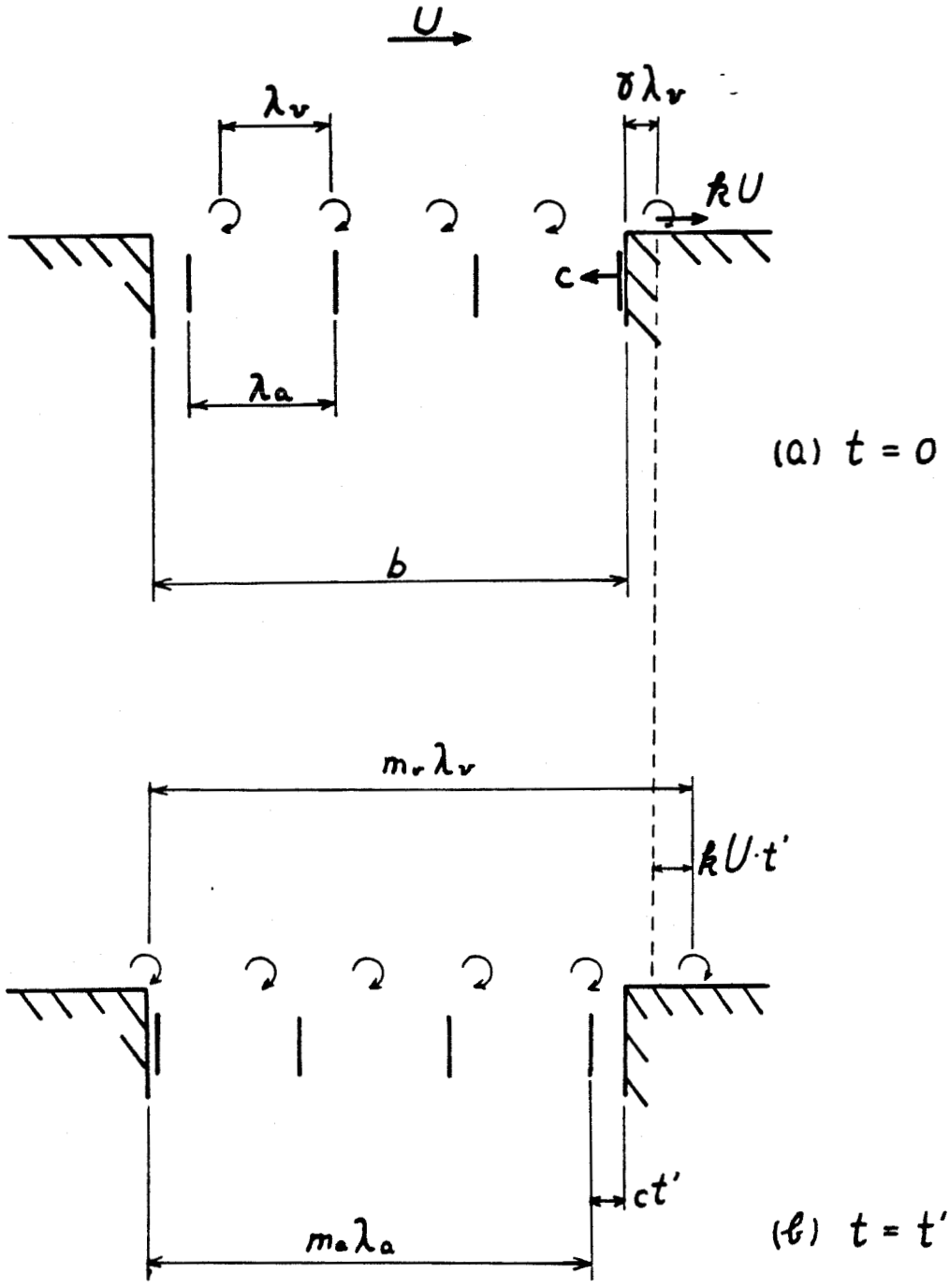

Fig.2.4.1. Rossiter's Model on Vortex/Acoustic Wave Interaction in Cavity Flow.

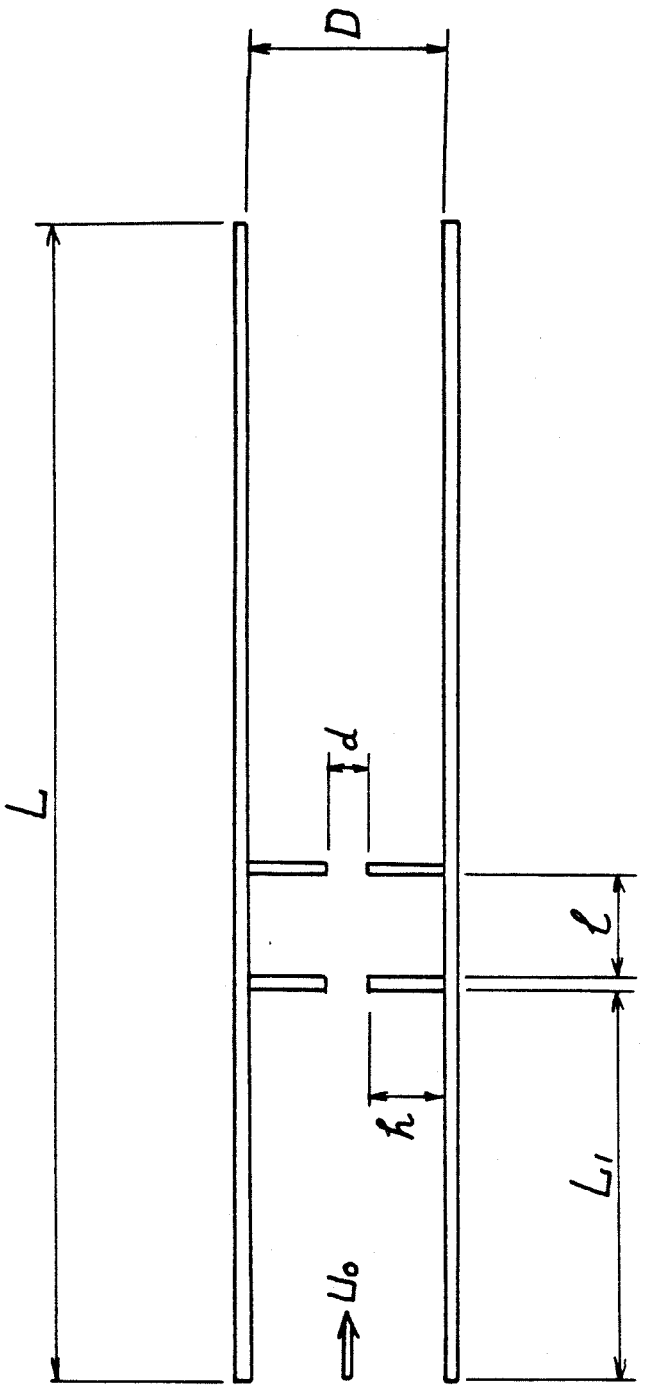

Fig.3.1. Internal Flow System.

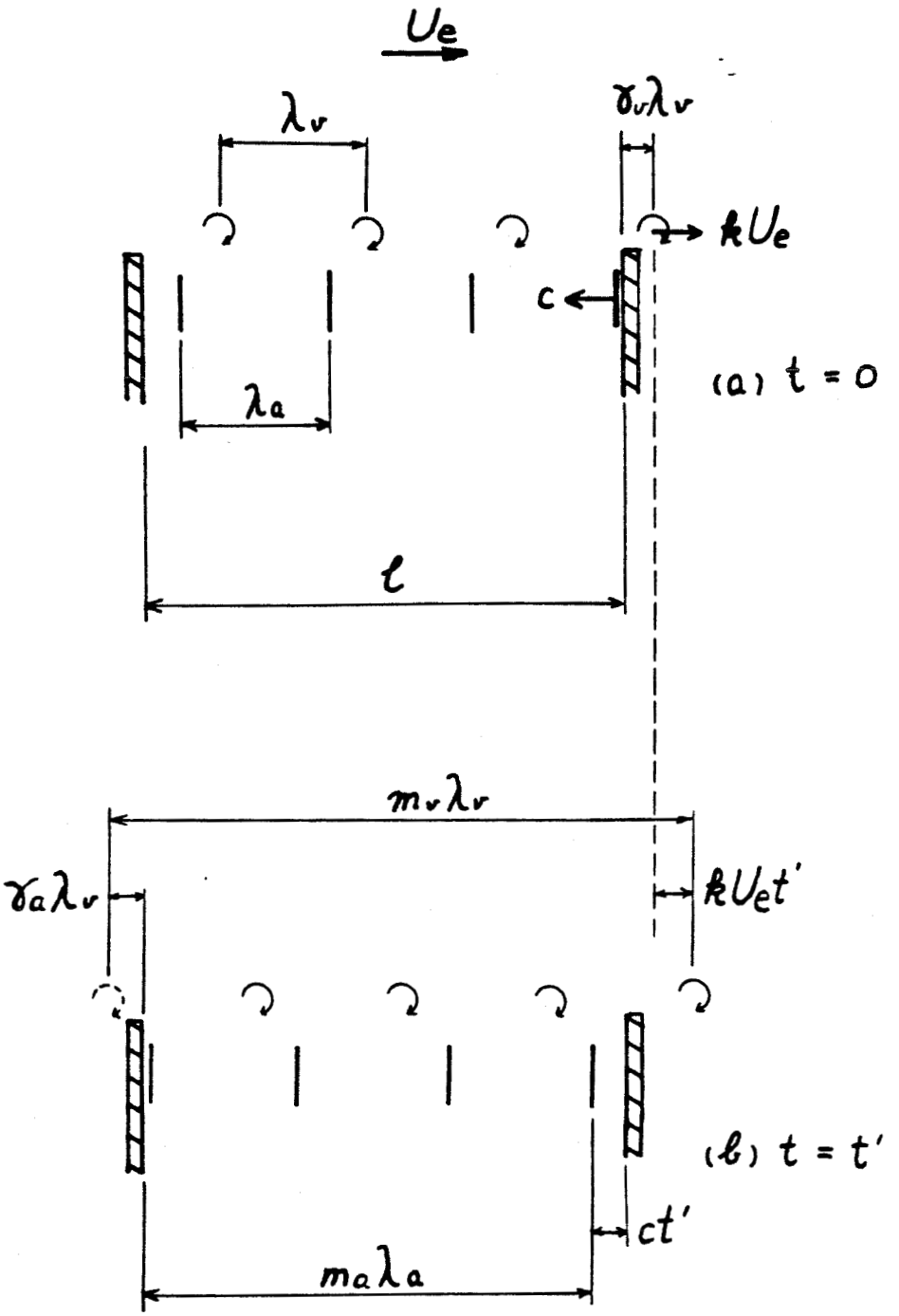

Fig.3.3.1. Vortex/Acoustic Wave Interaction Model.

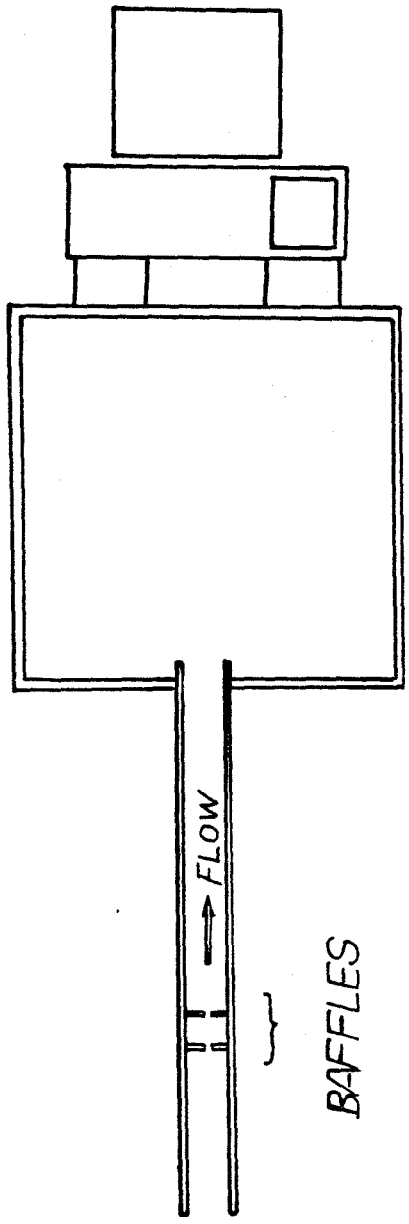

Fig.4.1.1. Schematic of the Apparatus.

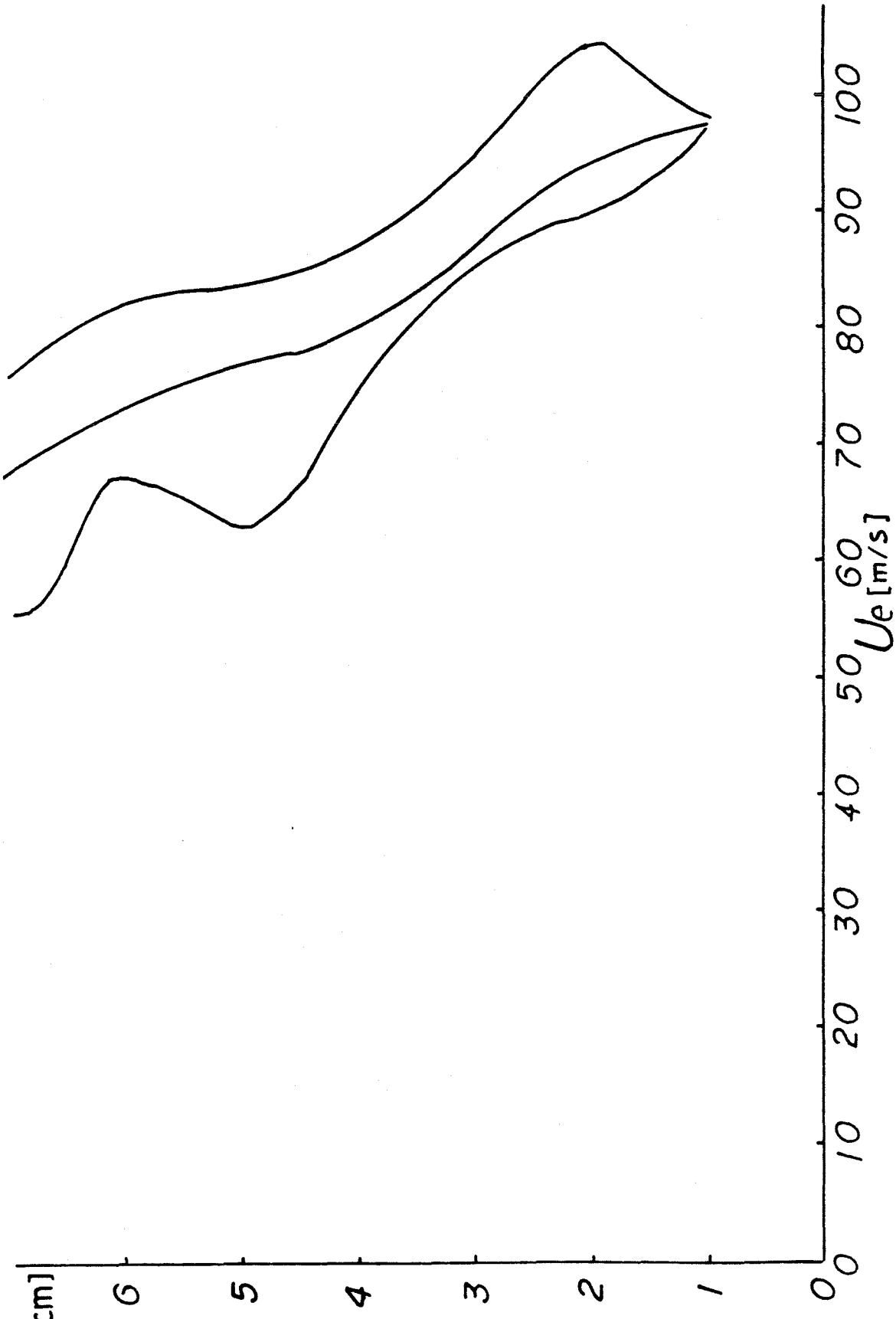

Fig.4.1.2. Blower Capability.

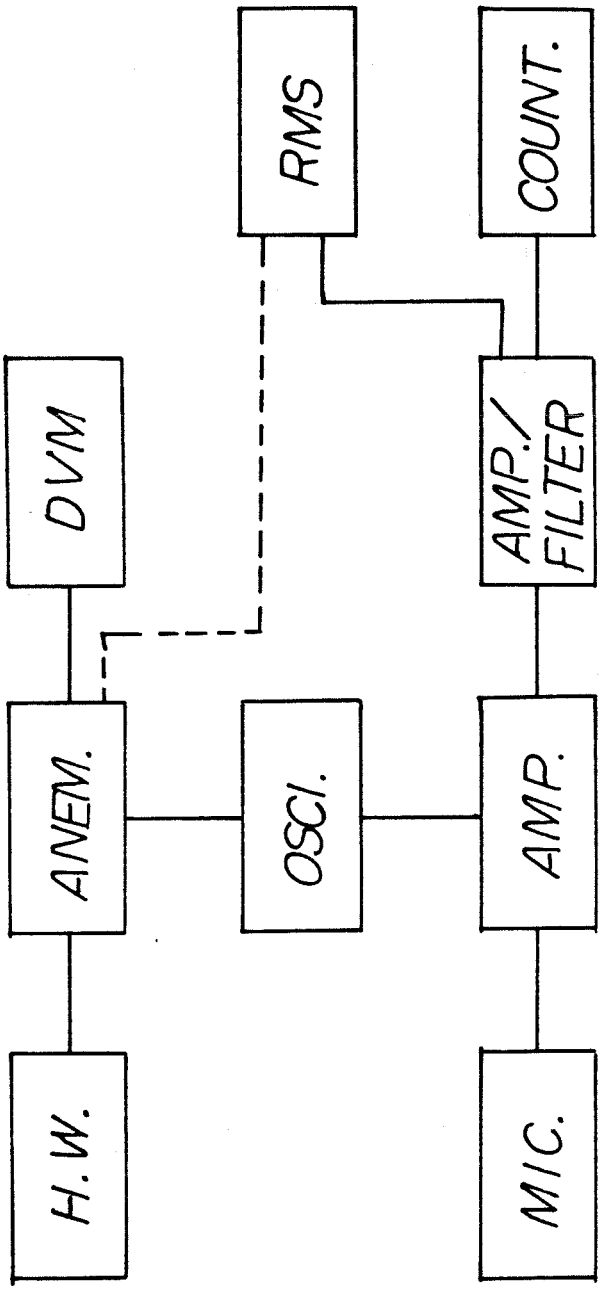

Fig.4.2.1. Measurement System.

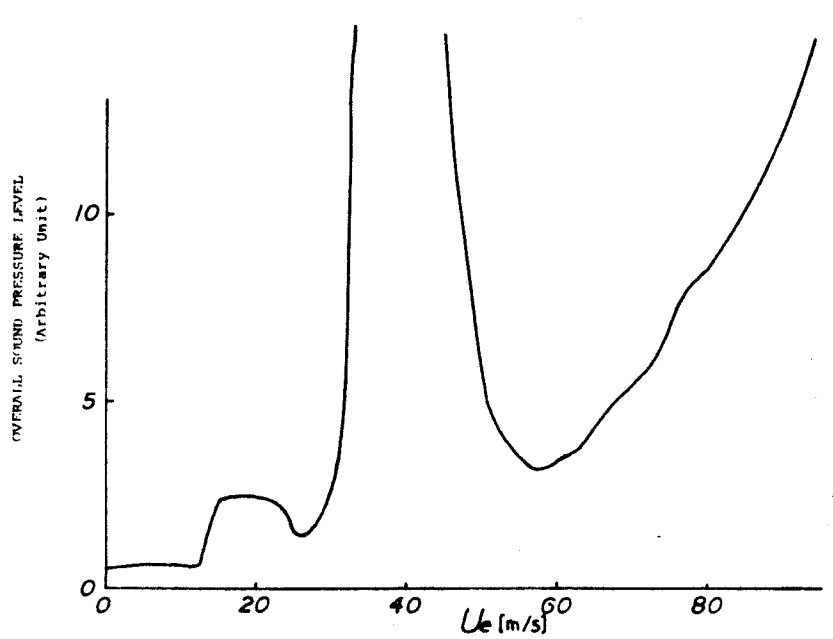

Fig.5.1.1. Overall Sound Pressure Level for l=1.0 cm.

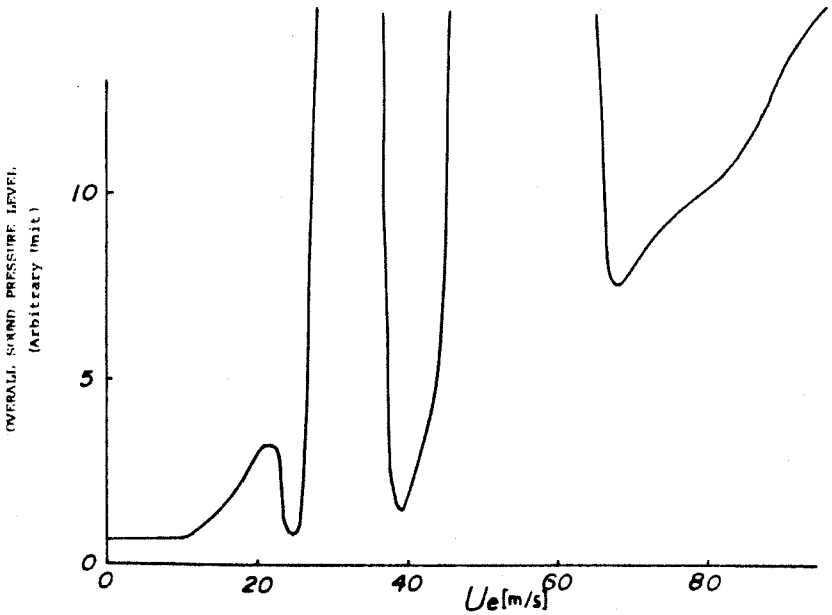

Fig.5.1.2. Overall Sound Pressure Level for l=2.0 cm.

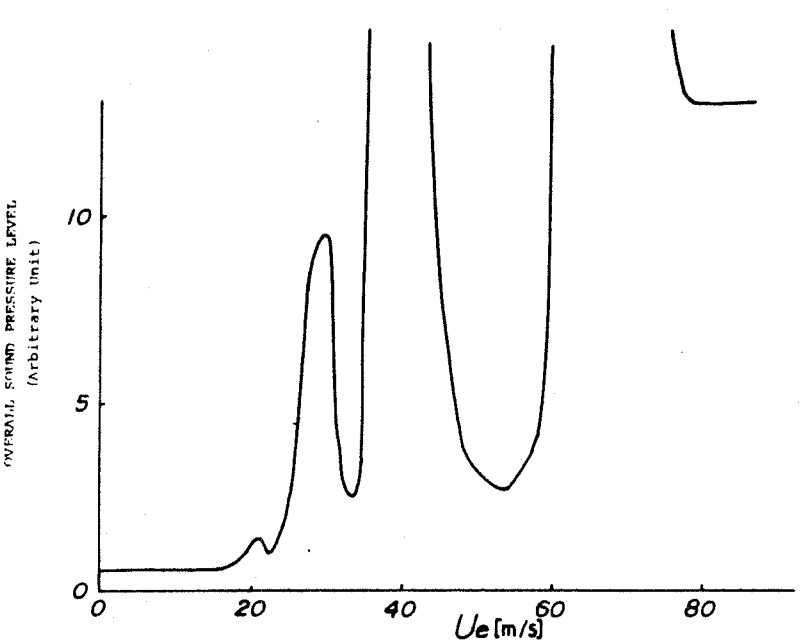

Fig.5.1.3. Overall Sound Pressure Level for l=3.0 cm.

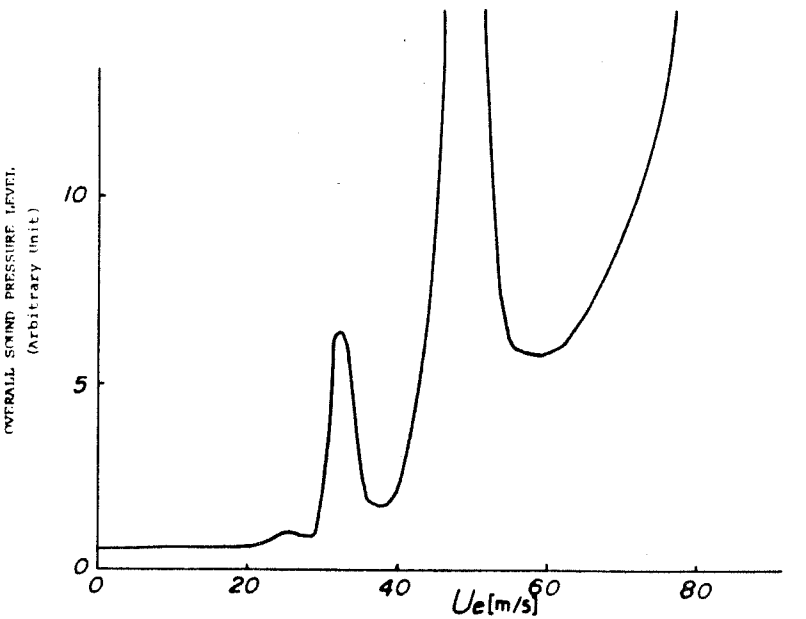

Fig.5.1.4. Overall Sound Pressure Level for l=4.0 cm.

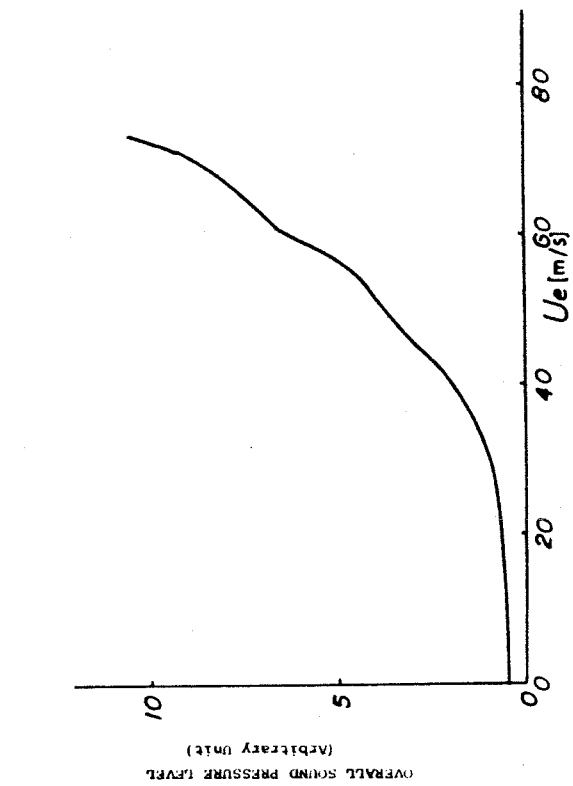

Fig.5.1.6. Overall Sound Pressure Level for l=6.0 cm.

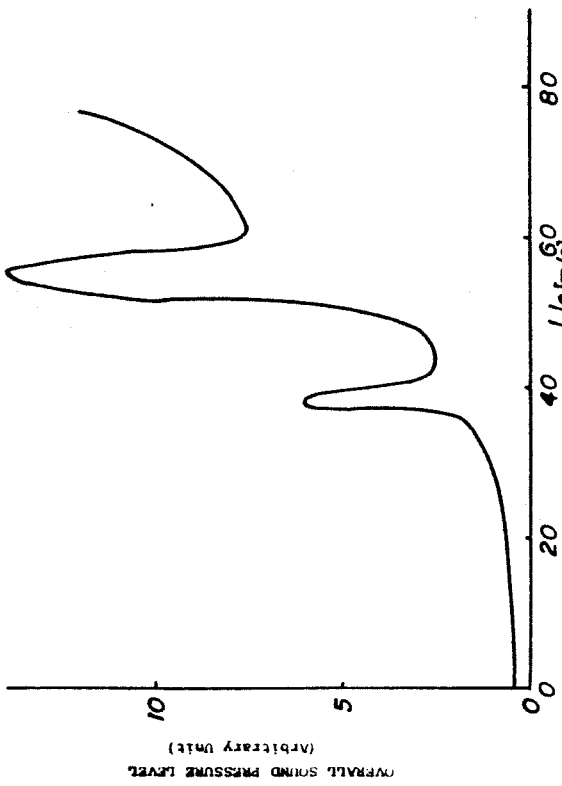

Fig.5.1.5. Overall Sound Pressure Level for l=5.0 cm.

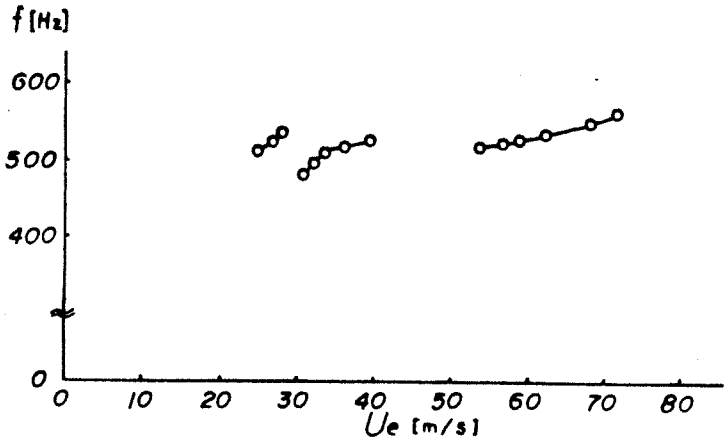

Fig.5.1.7. Resonant Frequency.
L=50.8 cm, L_1=20.0 cm, h=1.90 cm and l=3.0 cm.

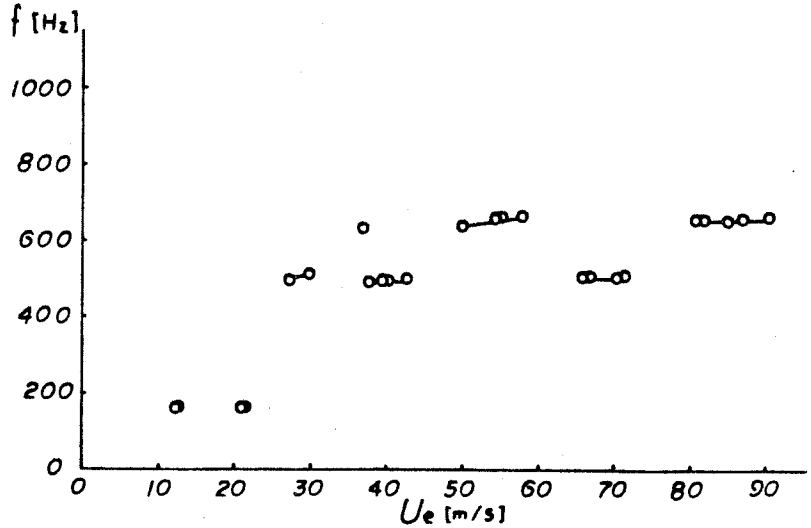

Fig.5.1.8. Resonant Frequency.
L=92.7 cm, L_1=20.0 cm, h=1.90 cm and l=3.0 cm.

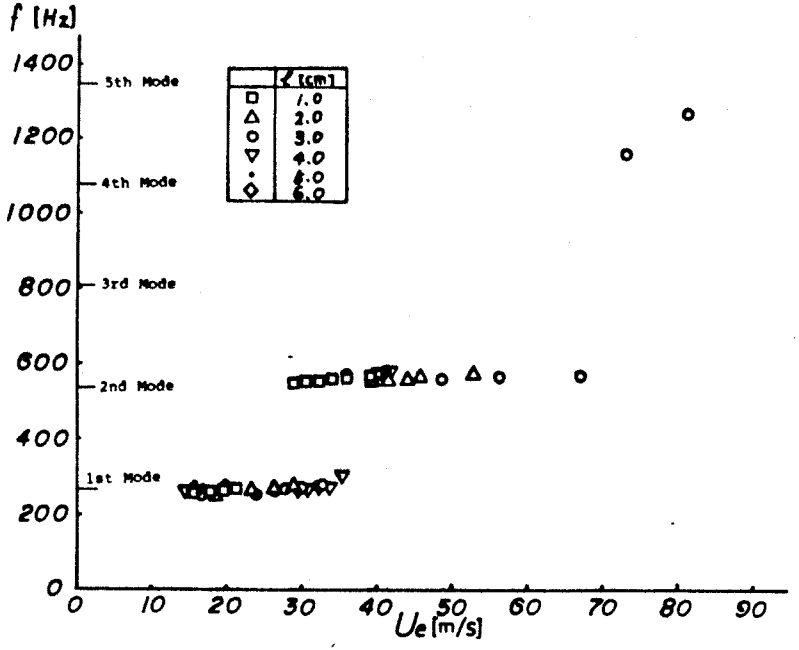

Fig.5.3.1. Resonant Frequency for L=50.8 cm, h=1.90 cm and L_1=1.0 cm.

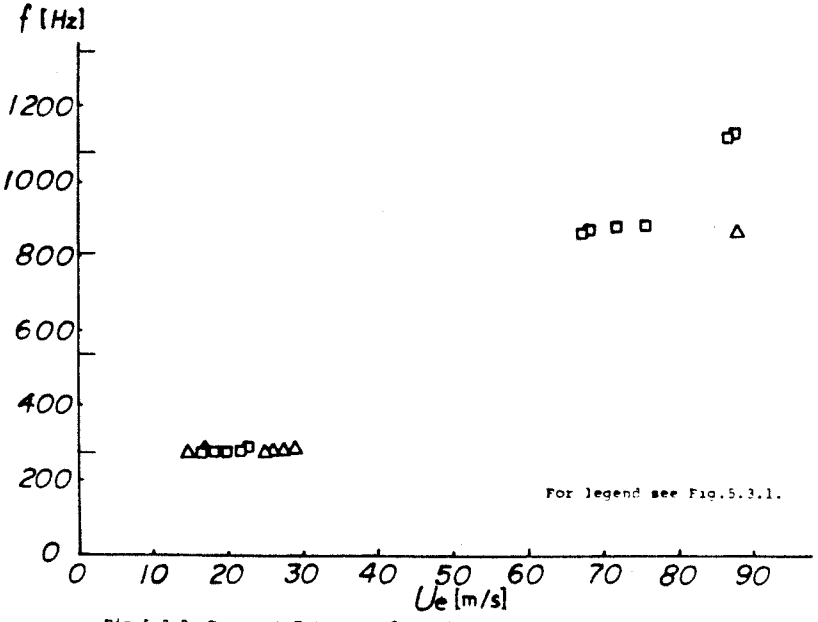

Fig.5.3.2. Resonant Frequency for L=50.8 cm, h=1.90 cm and L_1=10.0 cm.

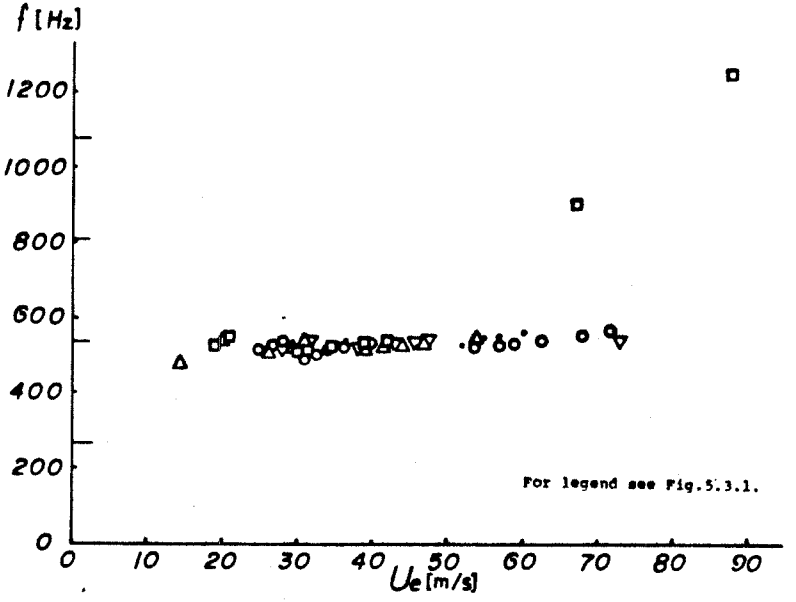

Fig.5.3.3. Resonant Frequency for L=50.8 cm, h=1.90 cm and L_1=20.0 cm.

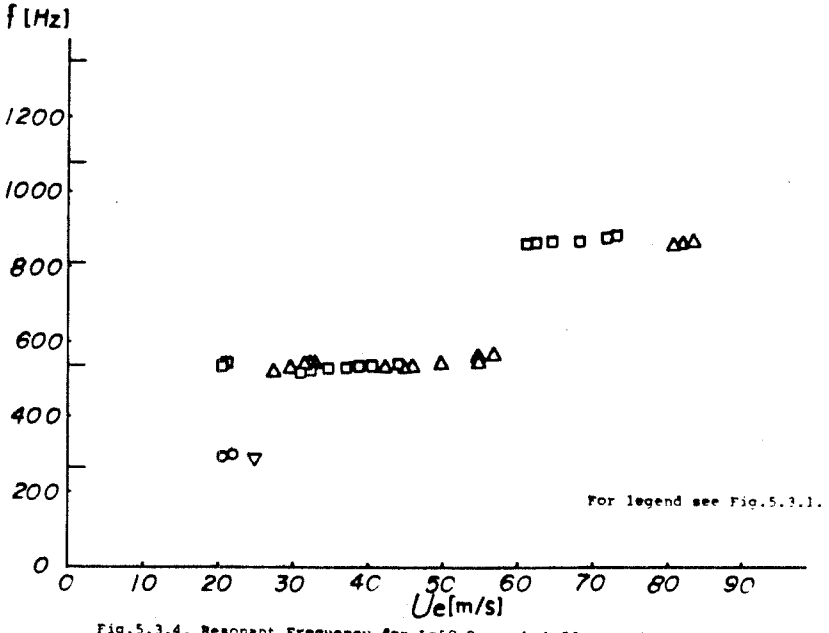

Fig.5.3.4. Resonant Frequency for L=50.8 cm, h=1.90 cm and L_1=30.0 cm.

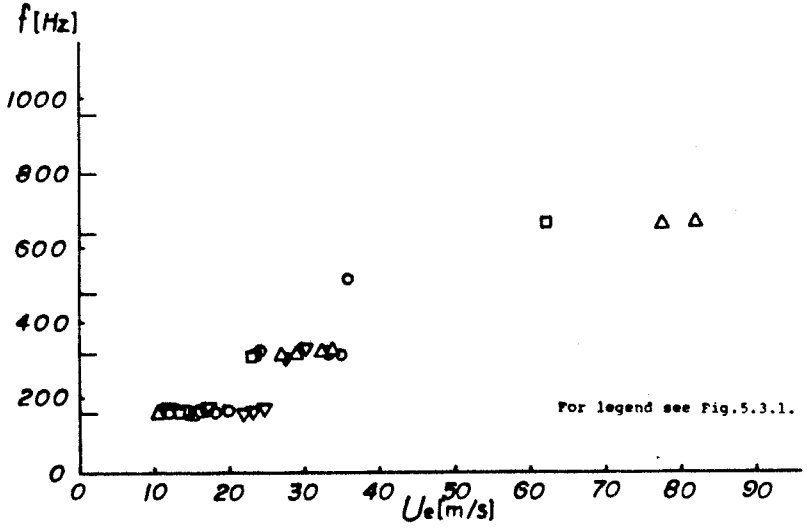

Fig.5.3.5. Resonant Frequency for L=92.7 cm, h=1.90 cm and L_1=1.0 cm.

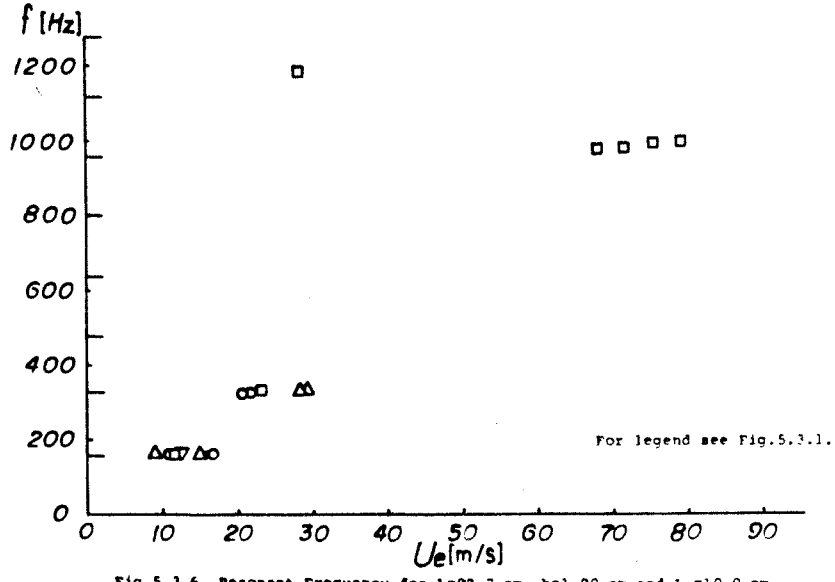

Fig.5.3.6. Resonant Frequency for L=92.7 cm, h=1.90 cm and L_1=10.0 cm.

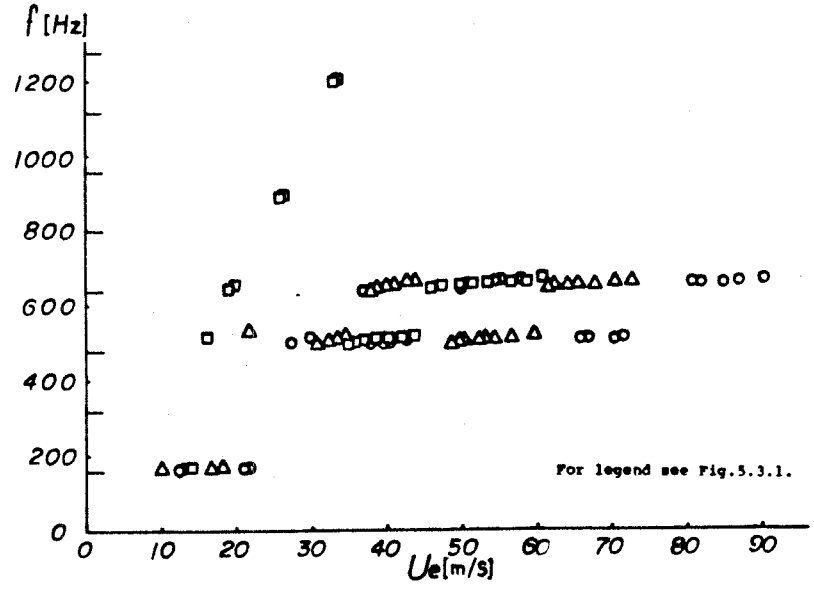

Fig.5.3.7. Resonant Frequency for L=92.7 cm, h=1.90 cm and L_1=20.0 cm.

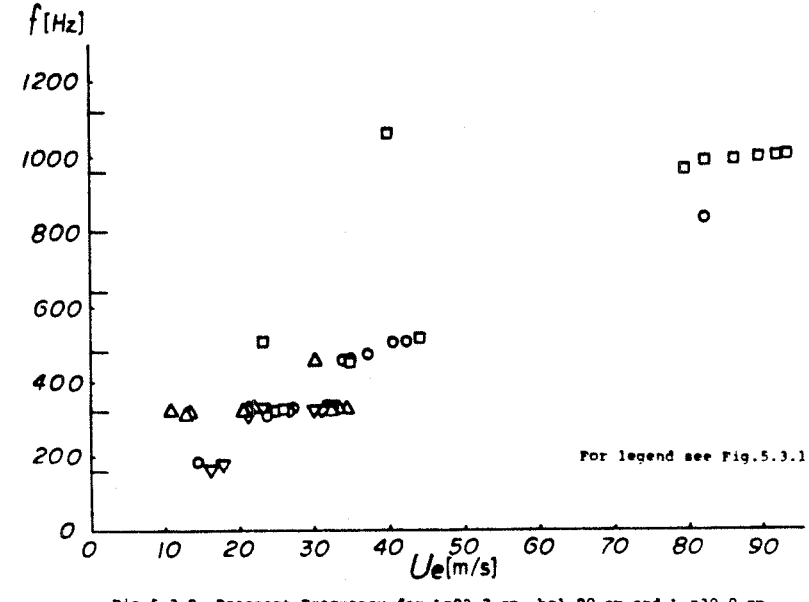

Fig.5.3.8. Resonant Frequency for L=92.7 cm, h=1.90 cm and L_1=30.0 cm.

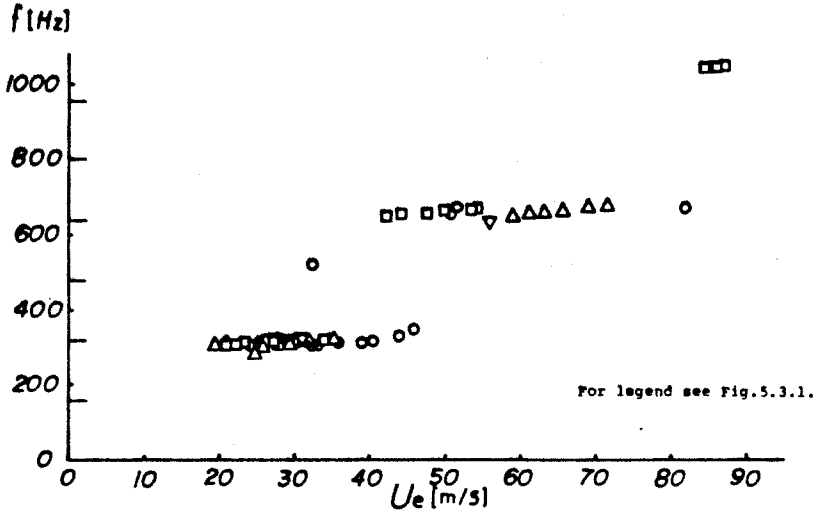

Fig.5.3.9. Resonant Frequency for L=92.7 cm, h=1.90 cm and L_1=42.9 cm.

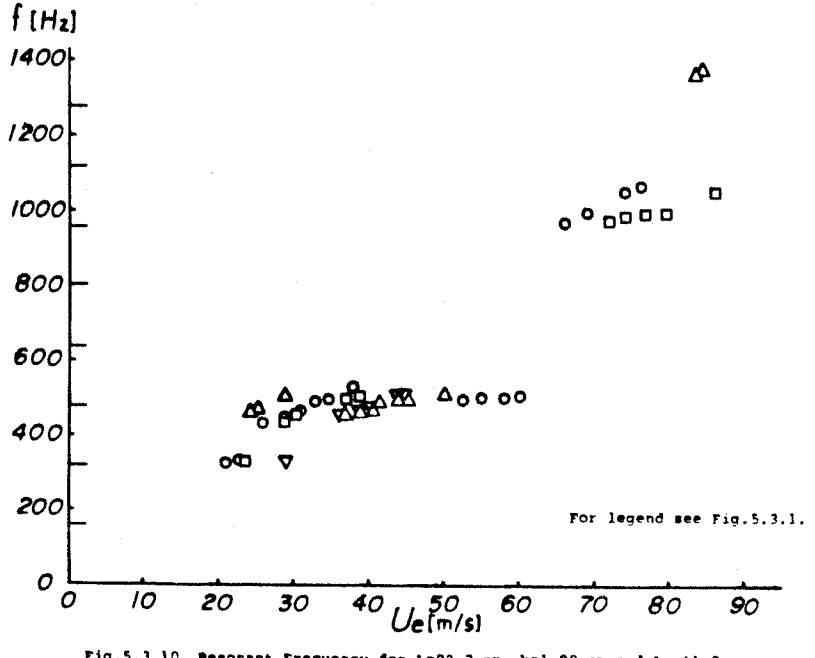

Fig.5.3.10. Resonant Frequency for L=92.7 cm, h=1.90 cm and L_1=61.9 cm.

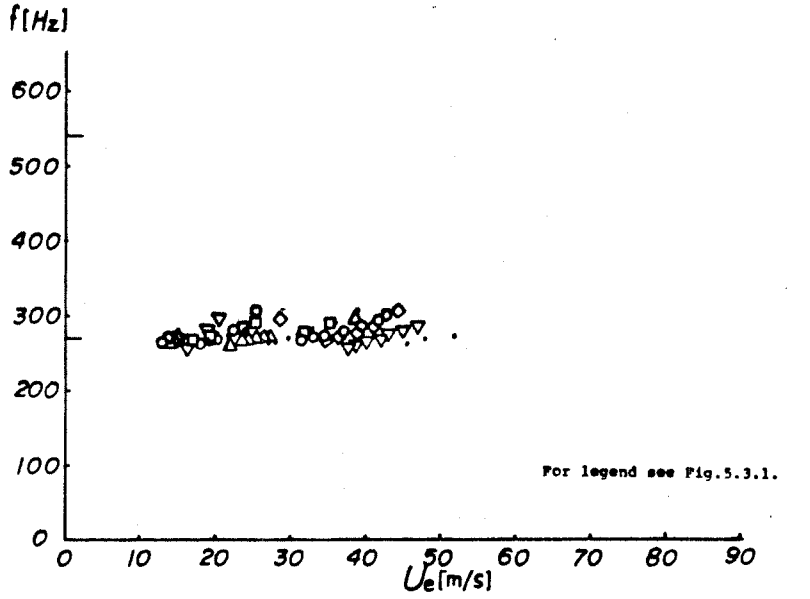

Fig.5.3.11. Resonant Frequency for L=50.8 cm, h=1.52 cm and L_1=1.0 cm.

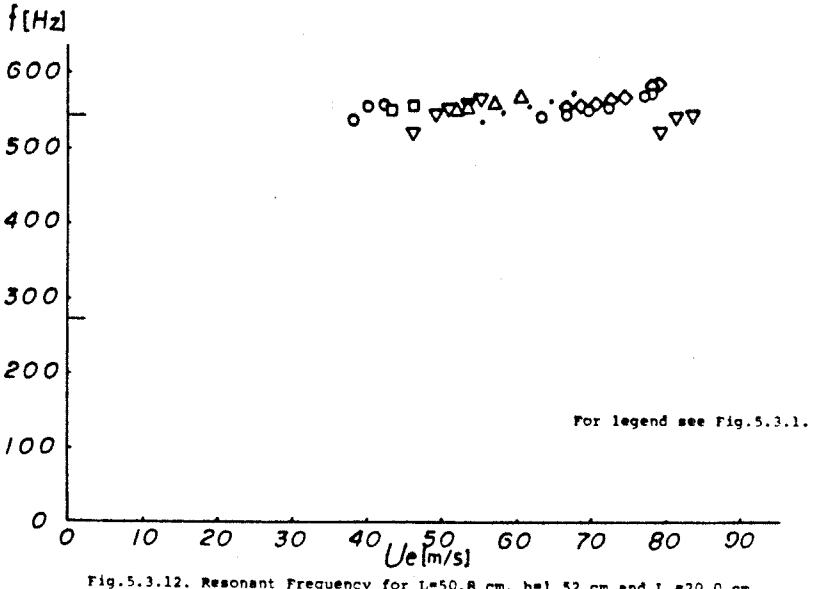

Fig.5.3.12. Resonant Frequency for L=50.8 cm, h=1.52 cm and L_1=20.0 cm.

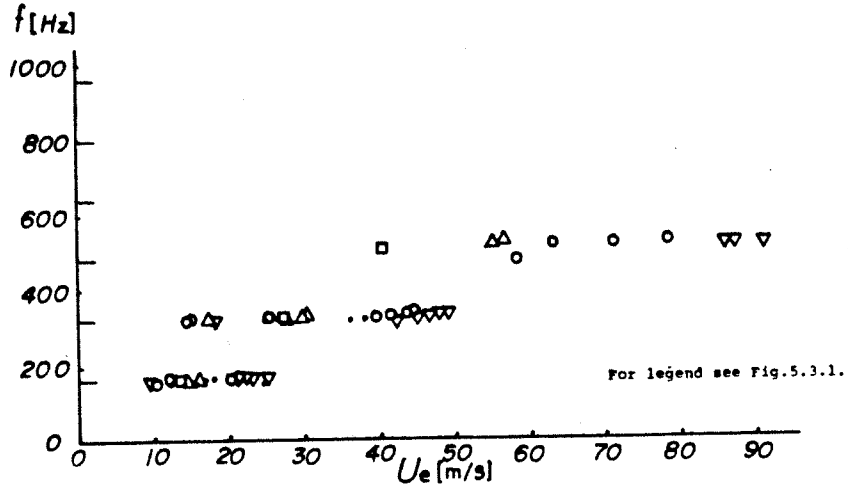

Fig.5.3.13. Resonant Frequency for L=92.7 cm, h=1.52 cm and L_1=1.0 cm.

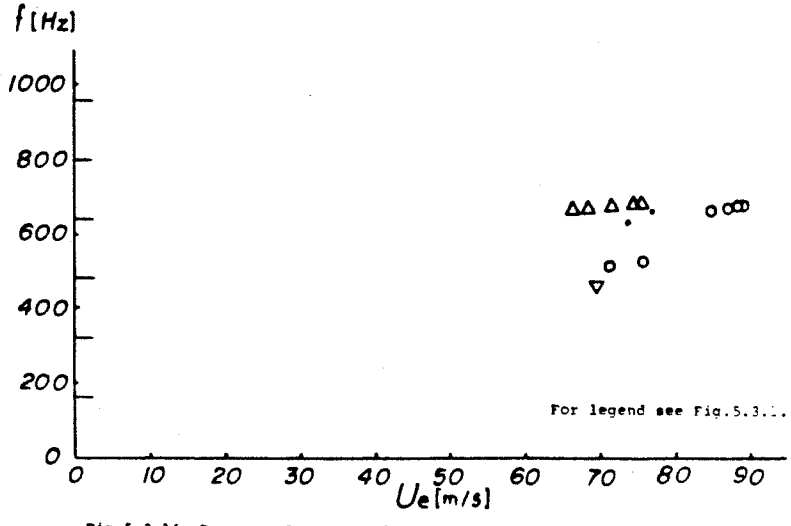

Fig.5.3.14. Resonant Frequency for L=92.7 cm, h=1.52 cm and L_1=20.0 cm.

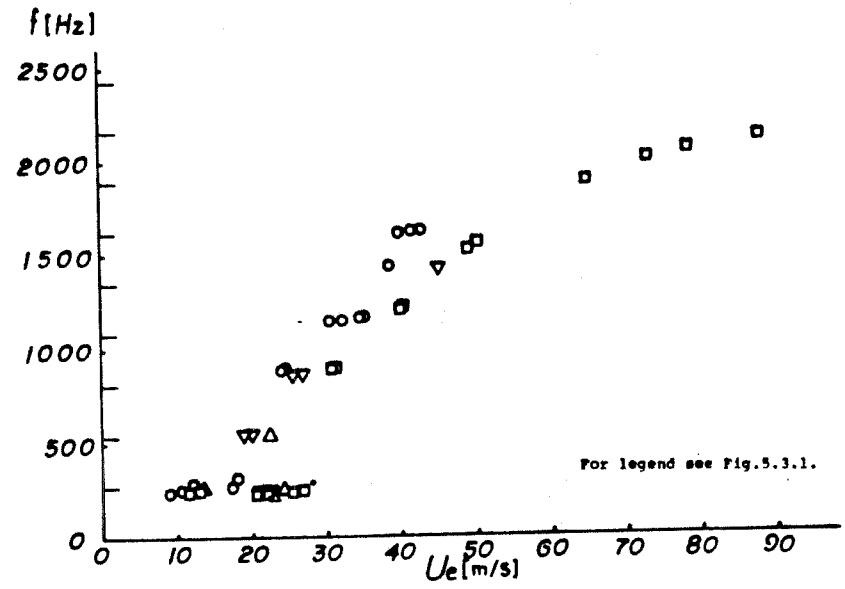

Fig.5.3.15. Resonant Frequency for L=50.8 cm, h=2.28 cm and L_1=1.0 cm.

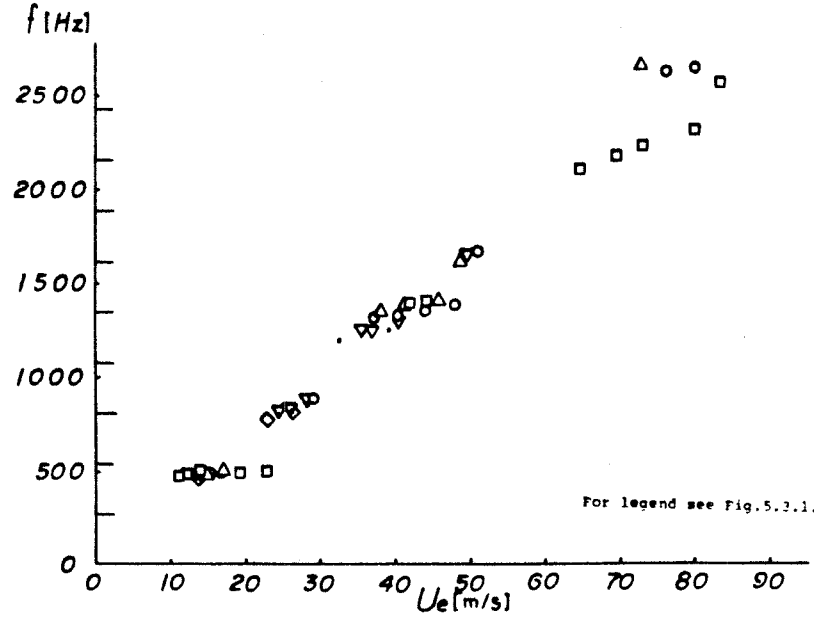

Fig.5.3.16. Resonant Frequency for L=50.8 cm, h=2.28 cm and L_1=20.0 cm.

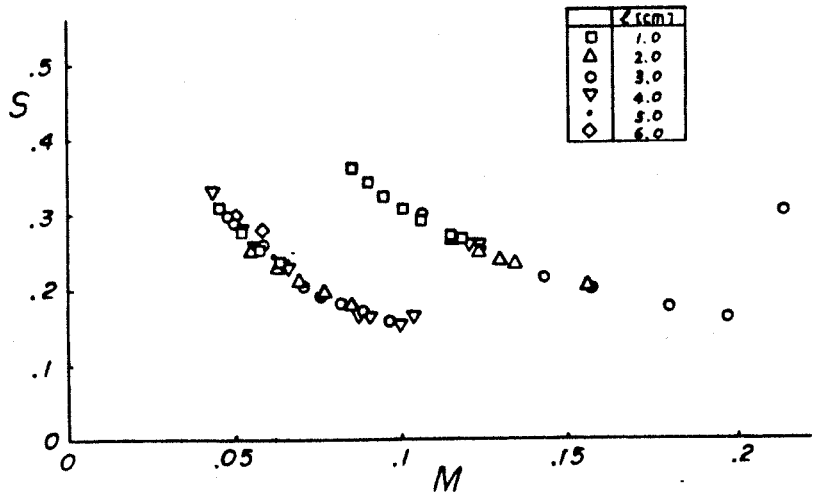

Fig.5.4.1. Strouhal Number for L=50.8 cm, h=1.90 cm and L_1=1.0 cm.

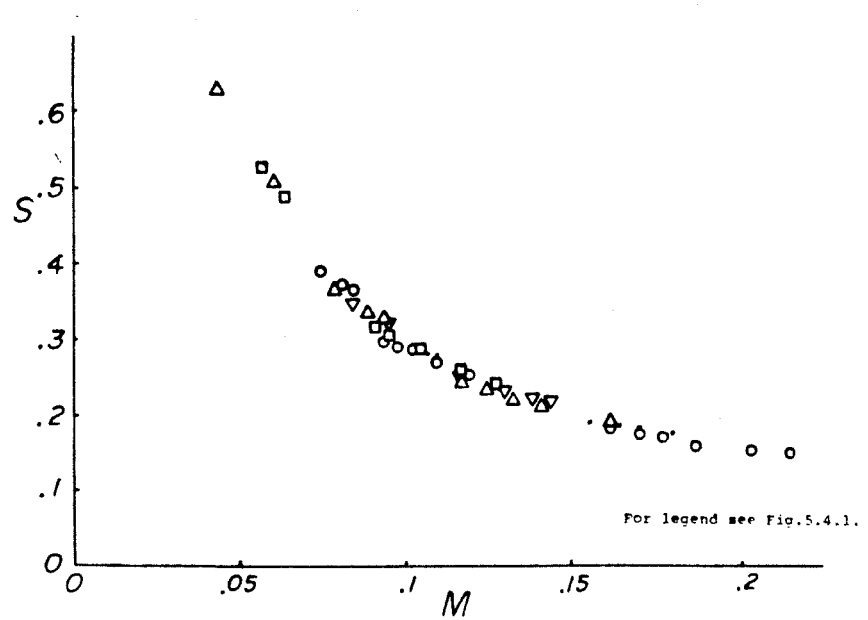

Fig.5.4.2. Strouhal Number for L=50.8 cm, h=1.90 cm and L_1=20.0 cm.

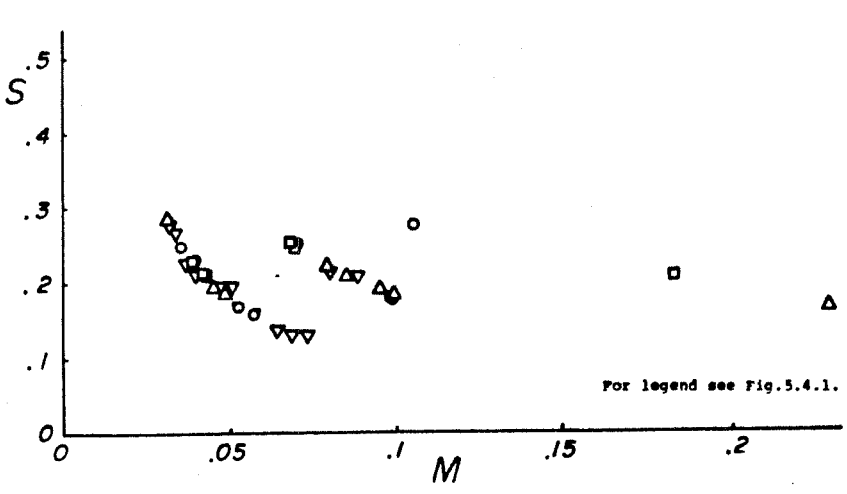

Fig.5.4.3. Strouhal Number for L=92.7 cm, h=1.90 cm and L_1=1.0 cm.

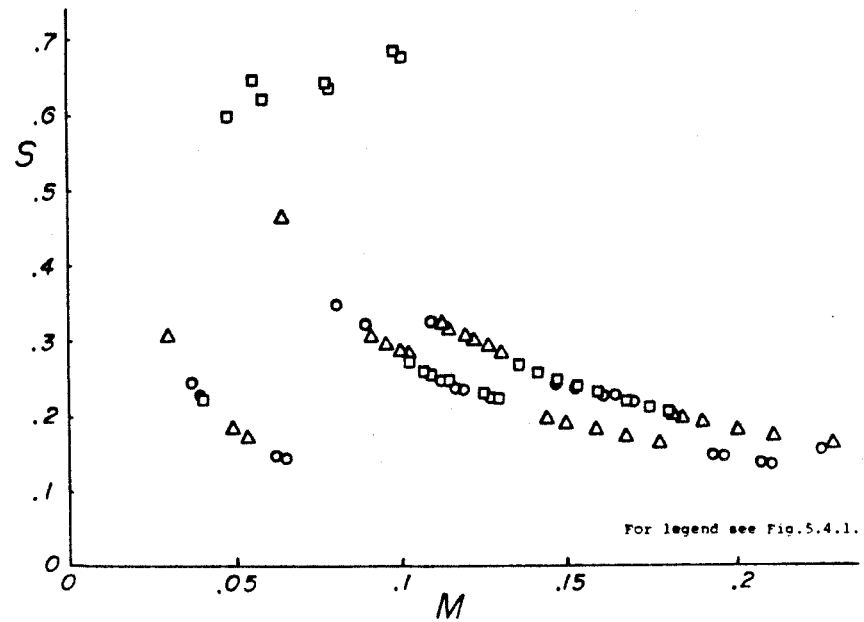

Fig.5.4.4. Strouhal Number for L=92.7 cm, h=1.90 cm and L_1=20.0 cm.

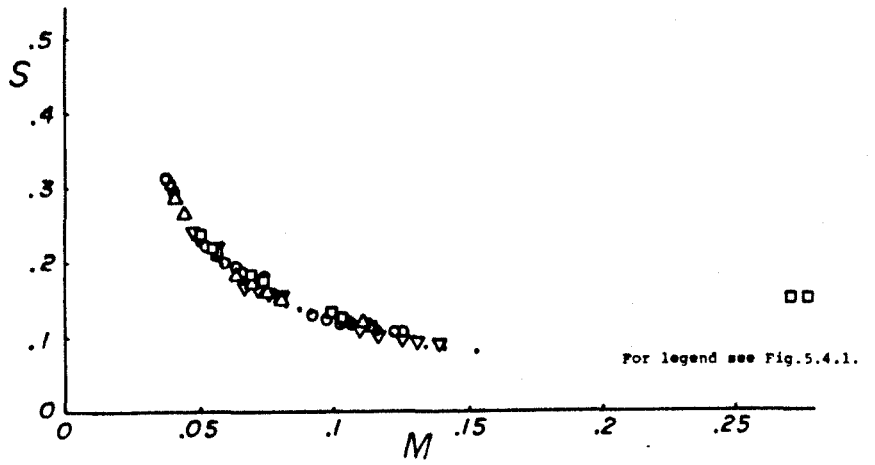

Fig.5.4.5. Strouhal Number for L=50.8 cm, h=1.52 cm and L_1=1.0 cm.

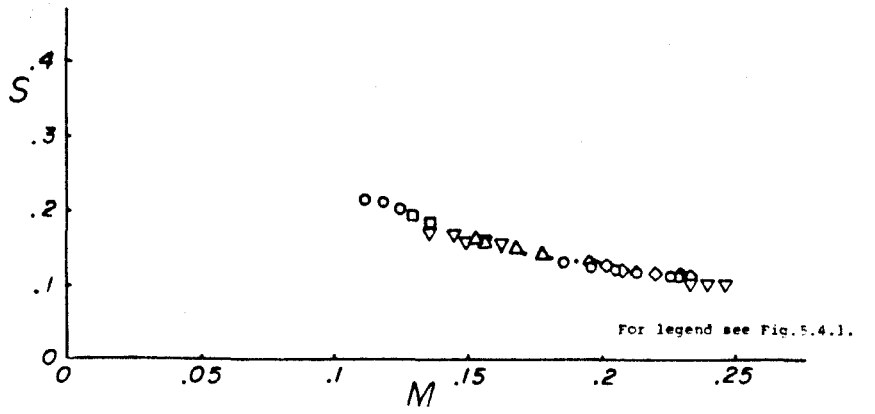

Fig.5.4.6. Strouhal Number for L=50.8 cm, h=1.52 cm and L_1=20.0 cm.

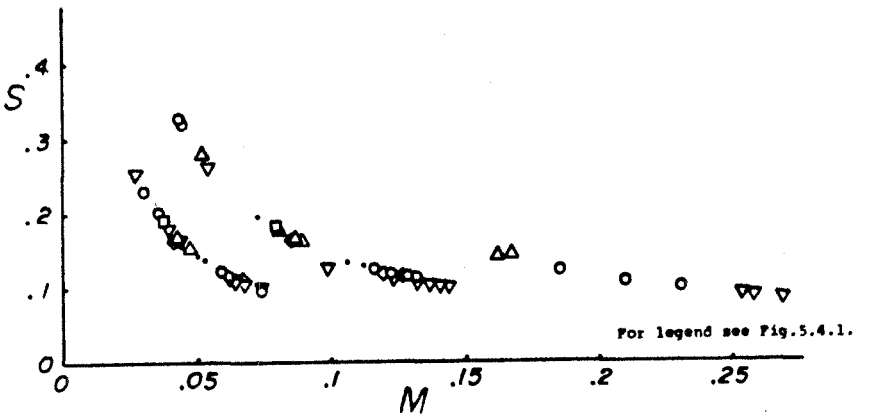

Fig.5.4.7. Strouhal Number for L=92.7 cm, h=1.52 cm and L_1=1.0 cm.

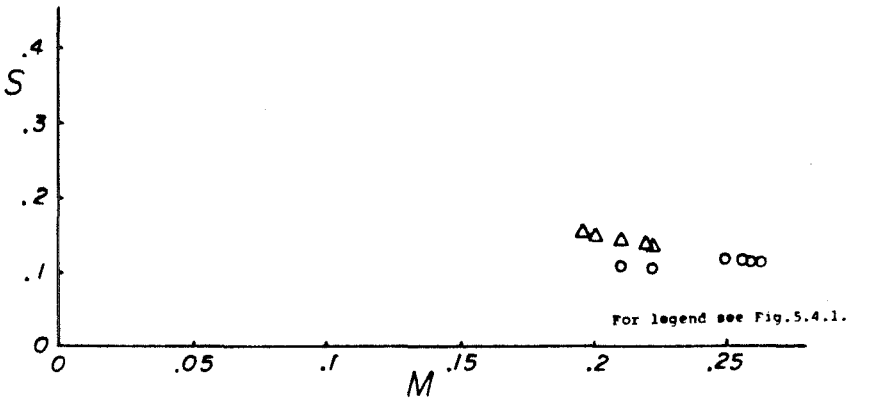

Fig.5.4.8. Strouhal Number for L=92.7 cm, h=1.52 cm and L_1=20.0 cm.

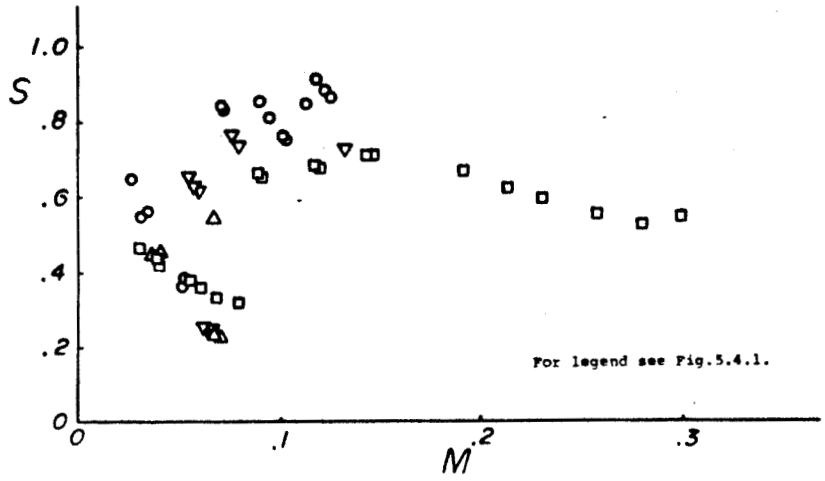

Fig.5.4.9. Strouhal Number for L=50.8 cm, h=2.28 cm and L_1=1.0 cm.

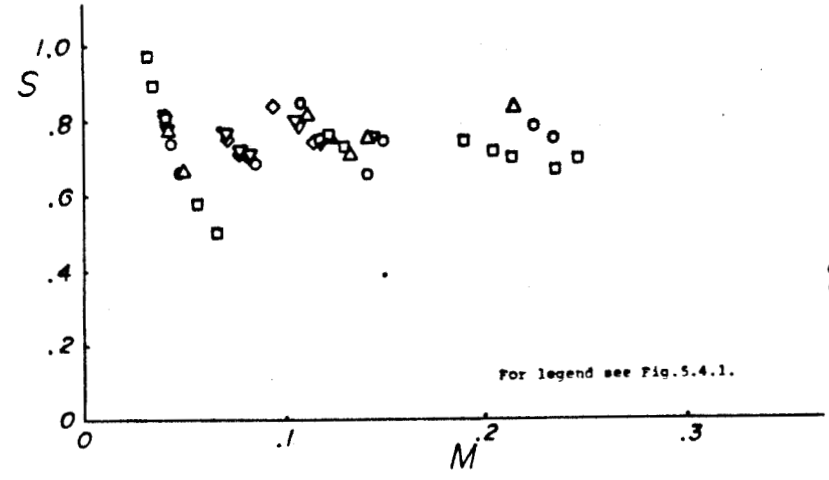

Fig.5.4.10. Strouhal Number for L=50.8 cm, h=2.28 cm and L_1=20.0 cm.

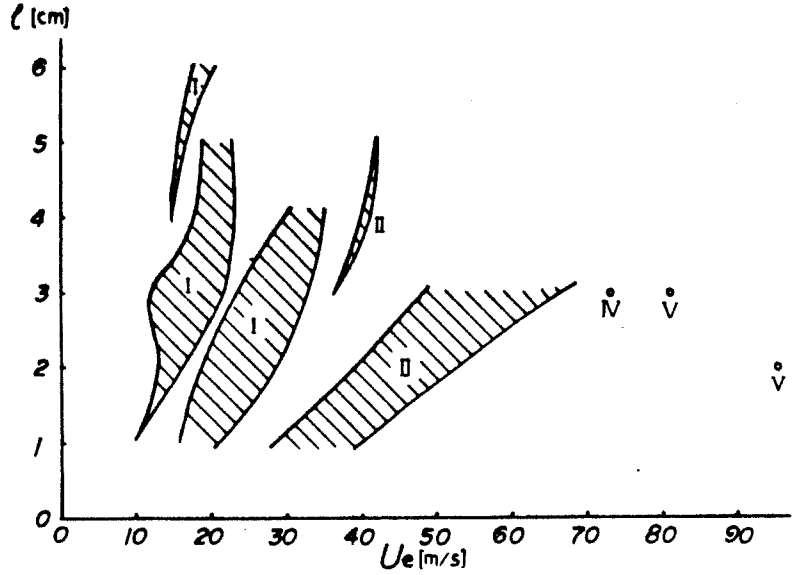

Fig.5.5.1. Pure Tine Production Regions for L=50.8 cm, h=1.90 cm and L_1=1.0 cm.

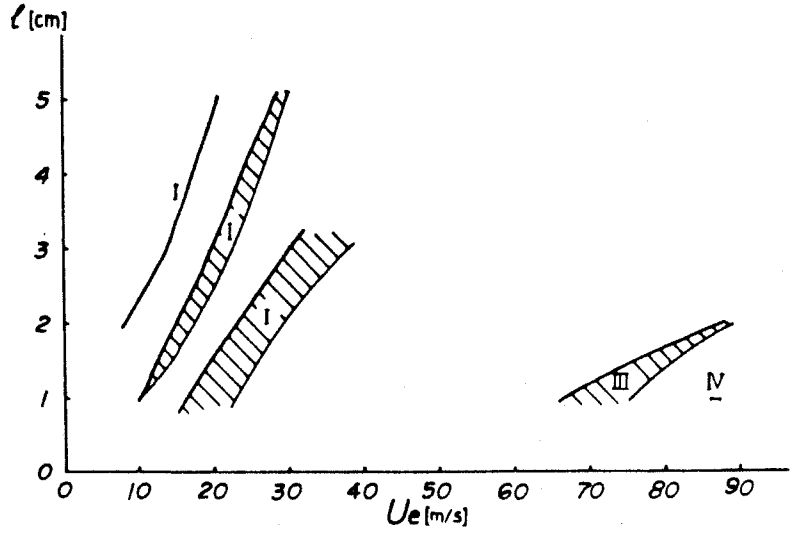

Fig.5.5.2. Pure Tone Production Regions for L=50.8 cm, h=1.90 cm and L_1=10.0 cm.

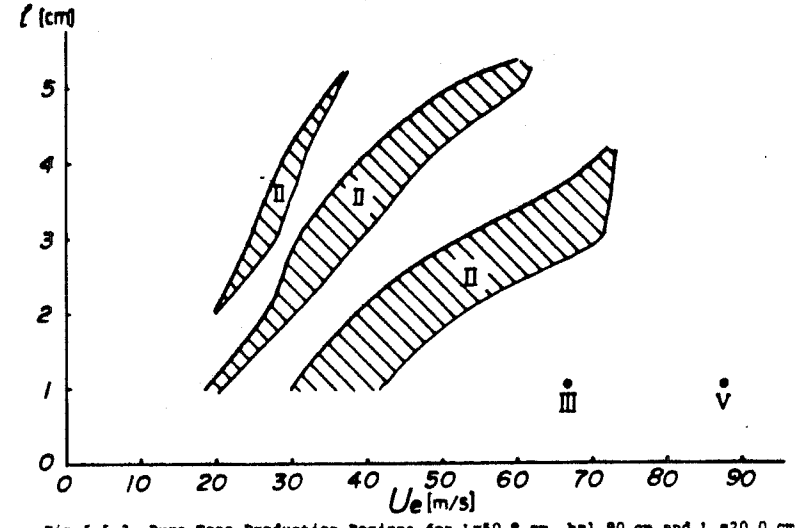

Fig.5.5.3. Pure Tone Production Regions for L=50.8 cm, h=1.90 cm and L_1=20.0 cm.

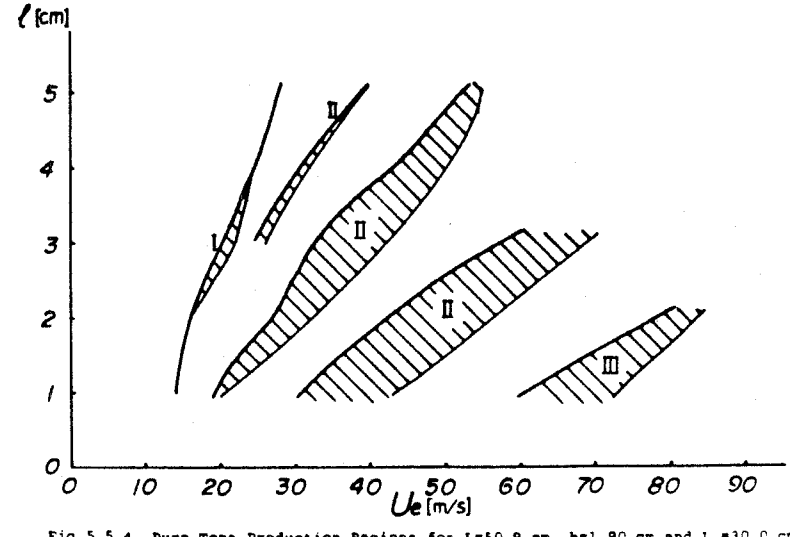

Fig.5.5.4. Pure Tone Production Regions for L=50.8 cm, h=1.90 cm and L_1=30.0 cm.

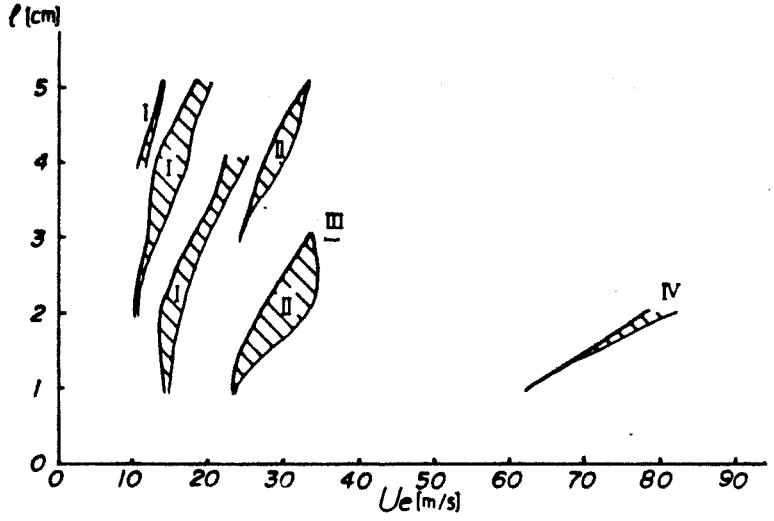

Fig.5.5.5. Pure Tone Production Regions for L=92.7 cm, h=1.90 cm and L_1=1.0 cm.

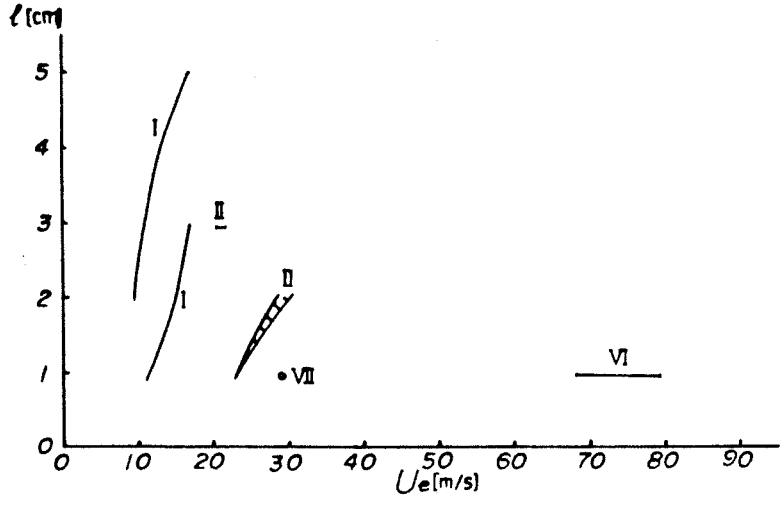

Fig.5.5.6. Pure Tone Production Regions for L=92.7 cm, h=1.90 cm and L_1=10.0 cm.

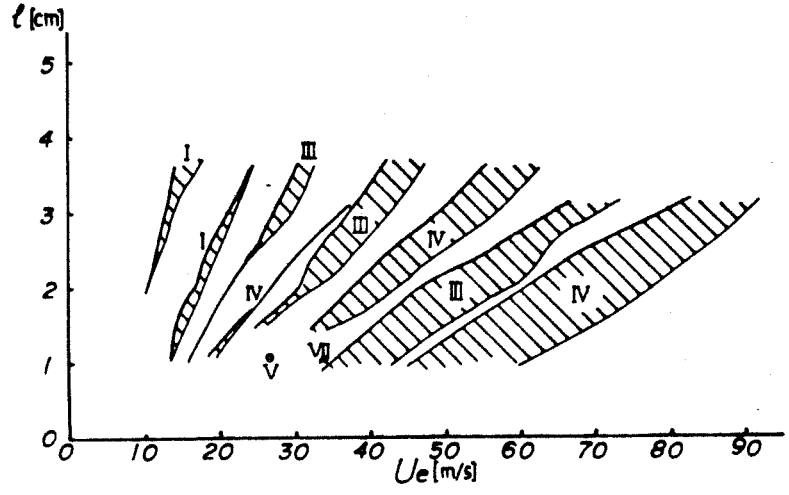

Fig.5.5.7. Pure Tone Production Regions for L=92.7 cm, h=1.90 cm and L_1=20.0 cm.

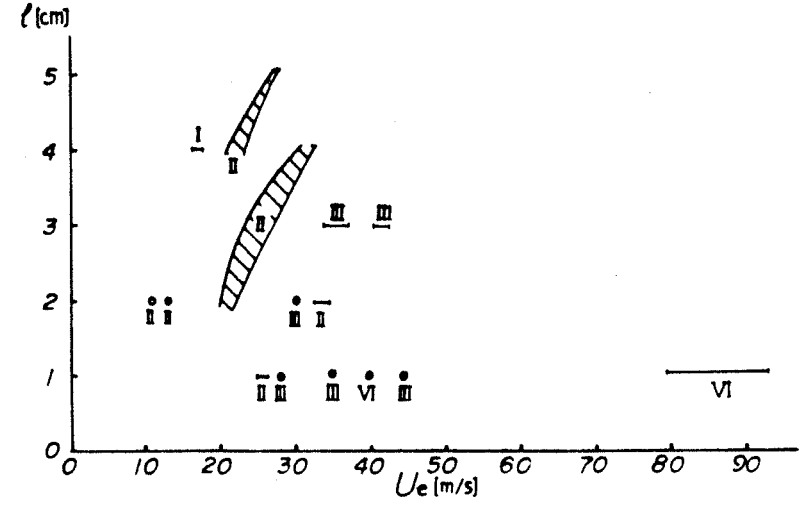

Fig.5.5.8. Pure Tone Production Regions for L=92.7 cm, h=1.90 cm and L_1=30.0 cm.

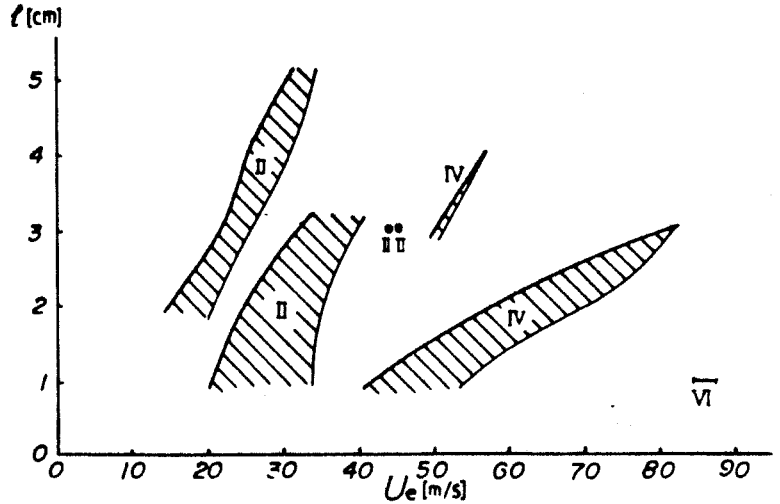

Fig.5.5.9. Pure Tone Production Regions for L=92.7 cm, h=1.90 cm and L_1=42.9 cm.

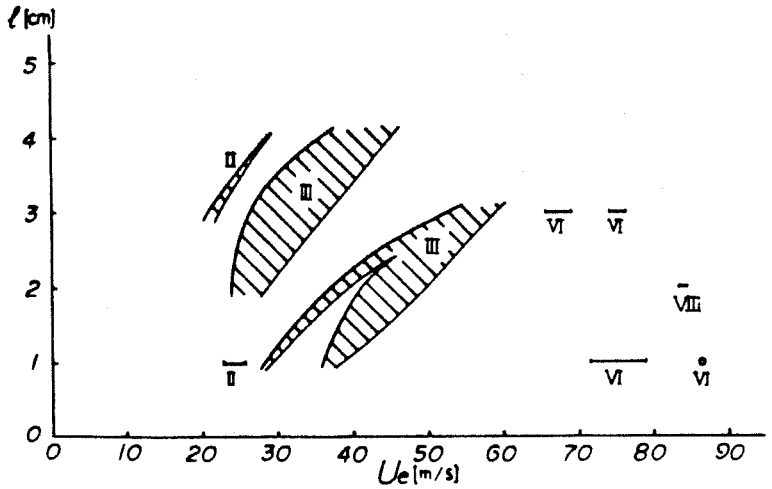

Fig.5.5.10. Pure Tone Production Regions for L=92.7 cm, h=1.90 cm and L_1=61.9 cm.

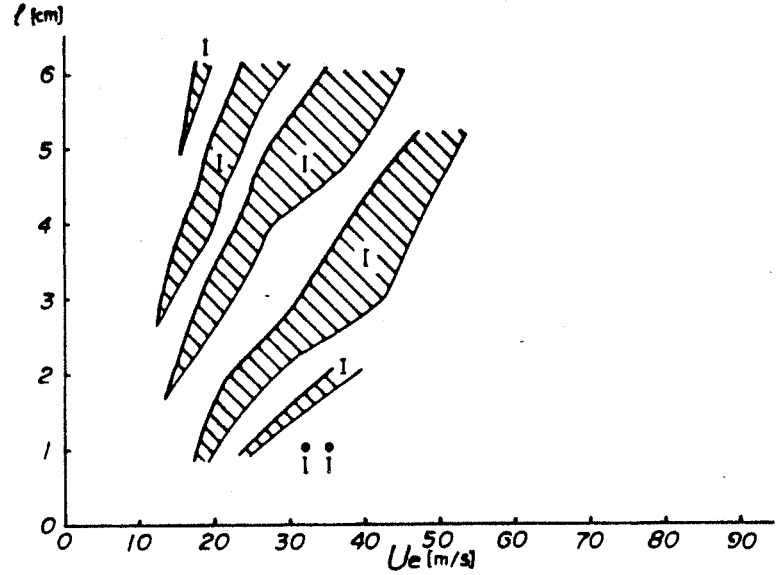

Fig.5.5.11. Pure Tone Production Regions for L=50.8 cm, h=1.52 cm and L_1=1.0 cm.

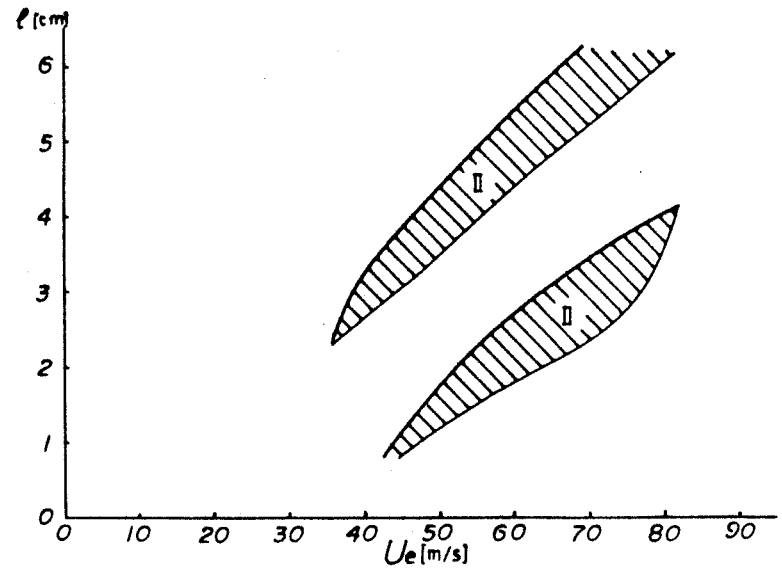

Fig.5.5.12. Pure Tone Production Regions for L=50.8 cm, h=1.52 cm and L_1=20.0 cm.

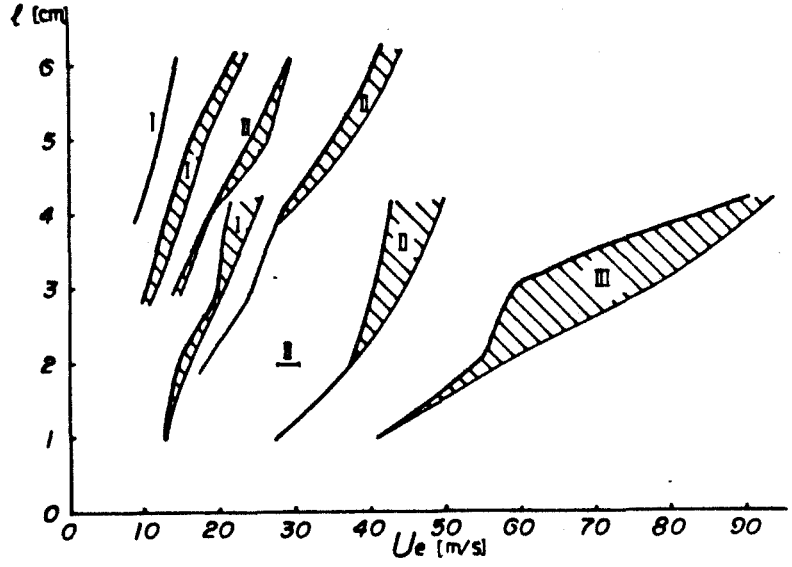

Fig.5.5.13. Pure Tone Production Regions for L=92.7 cm, h=1.52 cm and L_1=1.0 cm.

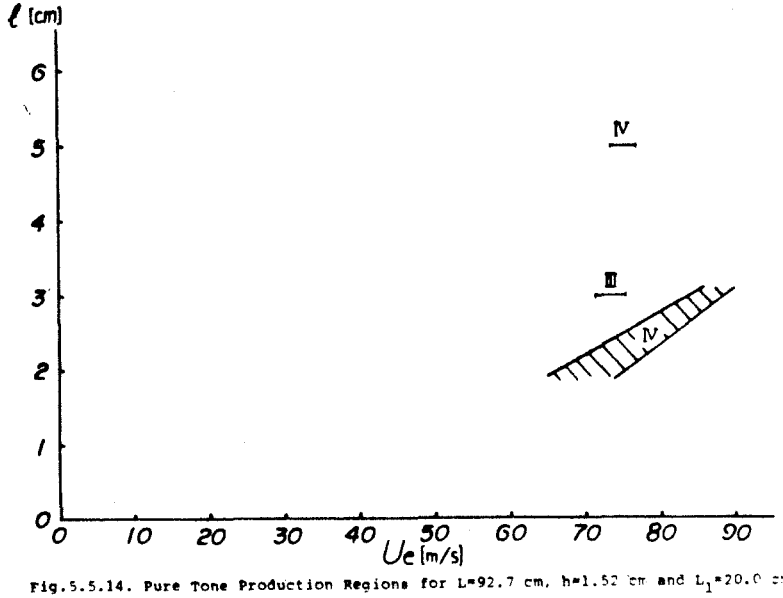

Fig.5.5.14. Pure Tone Production Regions for L=92.7 cm, h=1.52 cm and L_1=20.0 cm.

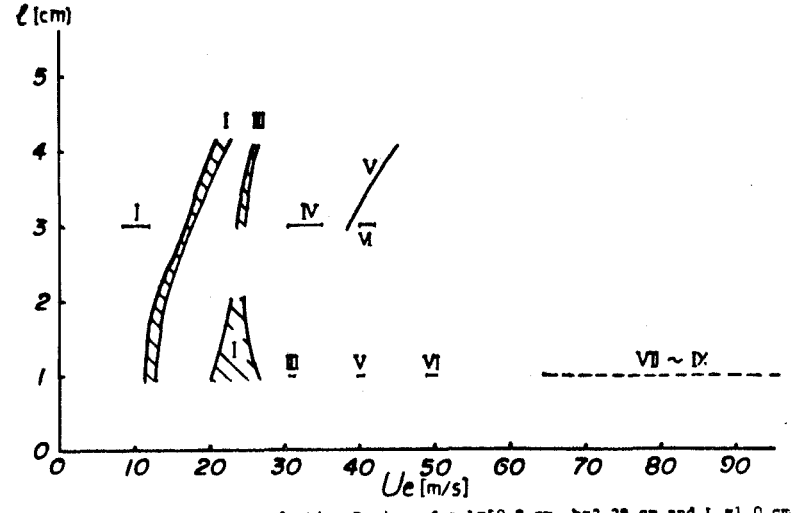

Fig.5.5.15. Pure Tone Production Regions for L=50.8 cm, h=2.28 cm and L_1=1.0 cm.

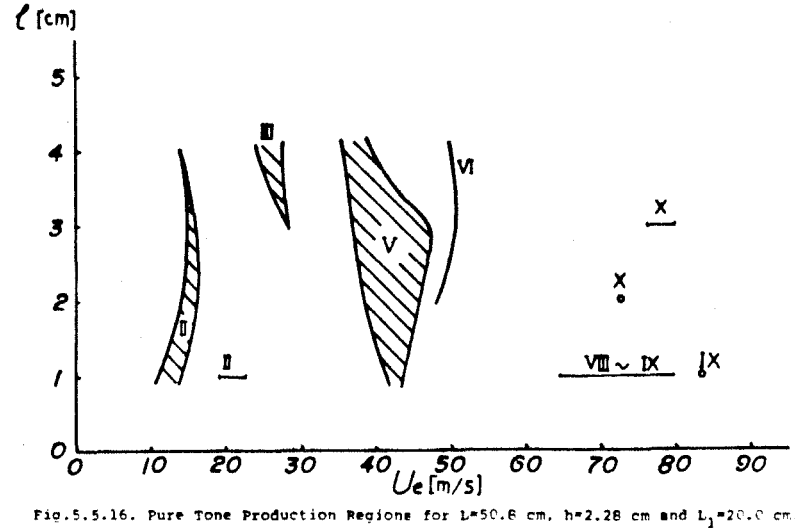

Fig.5.5.16. Pure Tone Production Regions for L=50.8 cm, h=2.28 cm and L_1=20.0 cm.

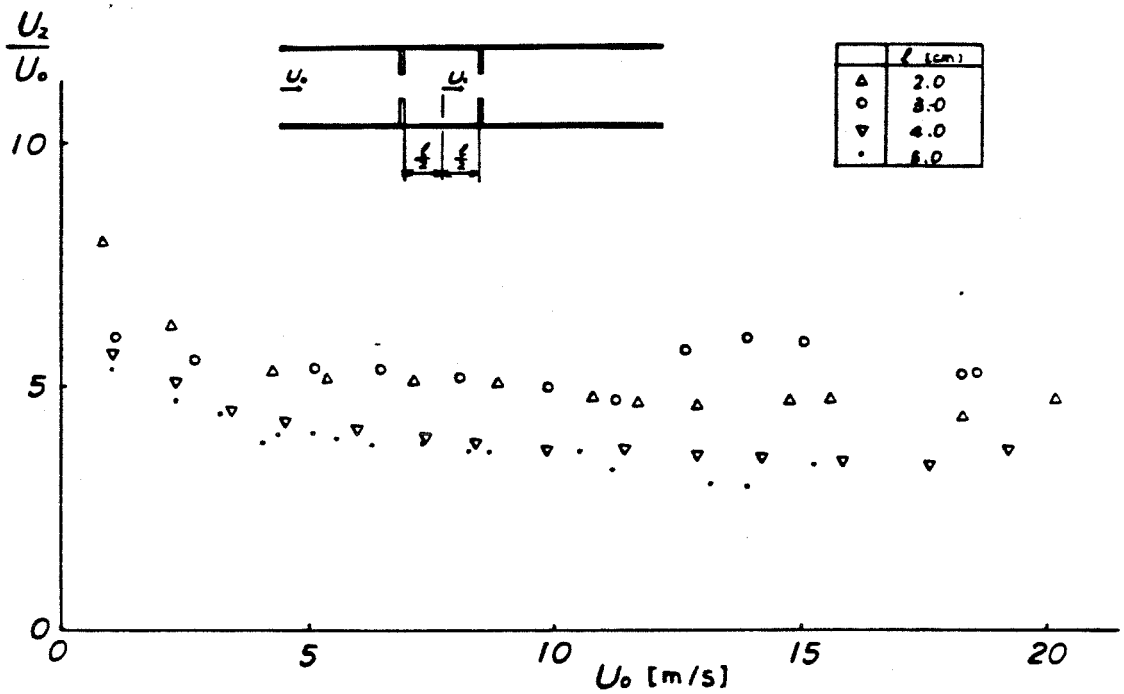

Fig.5.6.1. Centerline Flow Velocity Between the Baffles.
L=92.7 cm, L_1=20.0 cm and h=1.90 cm.

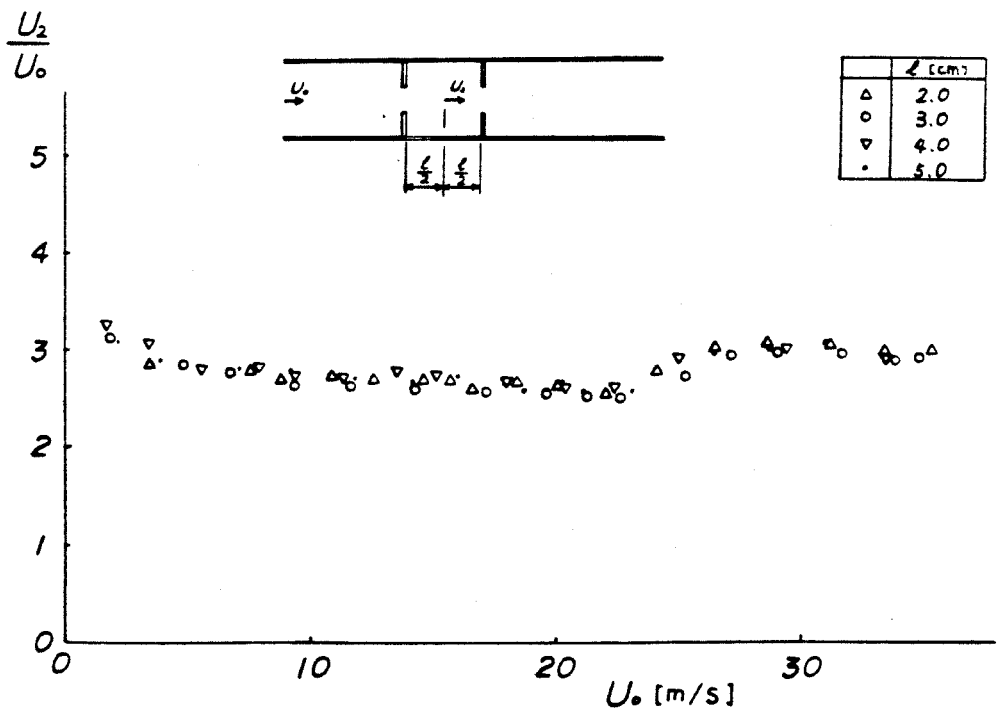

Fig.5.6.2. Centerline Flow Velocity Between the Baffles.
L=92.7 cm, L_1=20.0 cm and h=1.52 cm.

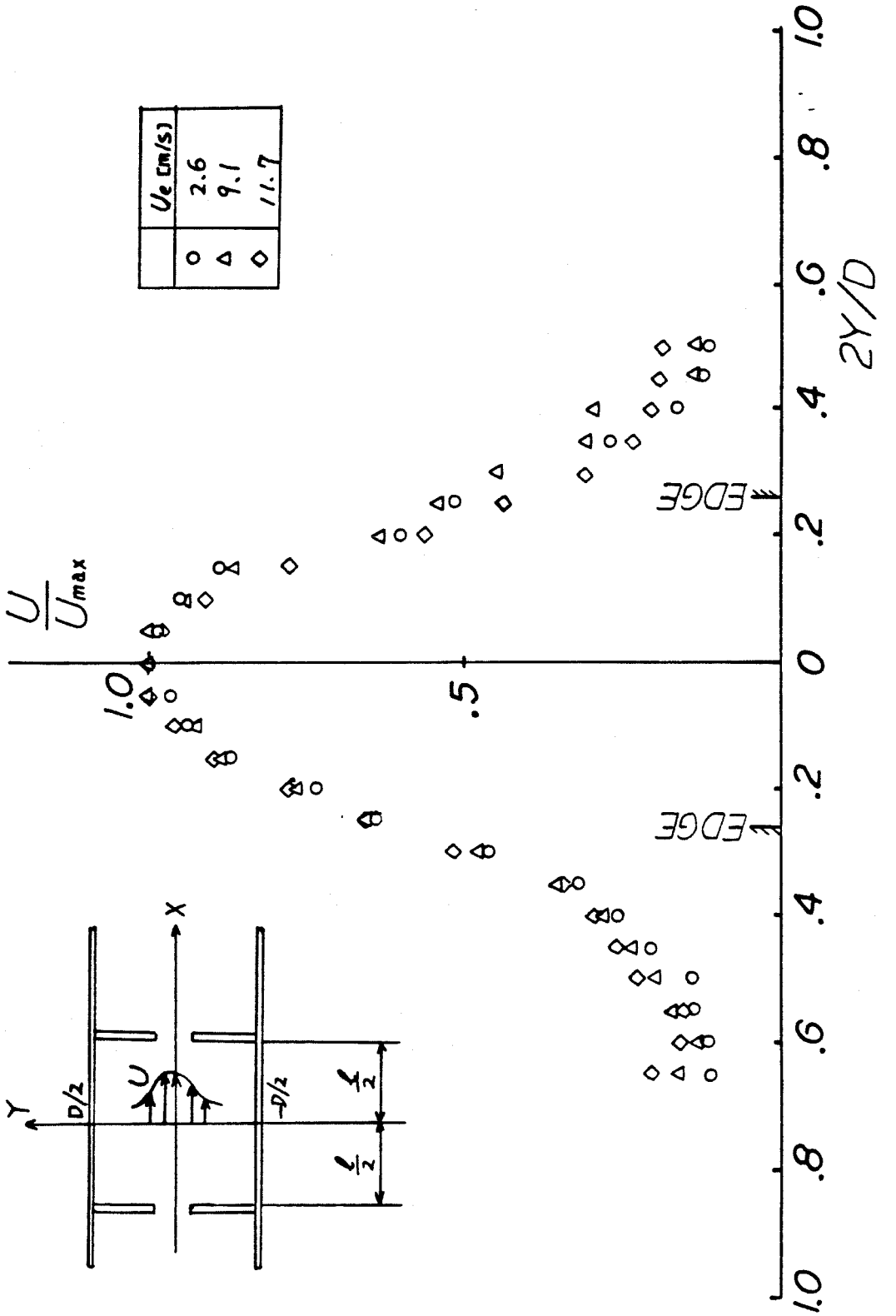

Fig.5.6.3. Velocity Profile Between the Baffles for h=1.90 cm and l=3.0 cm.

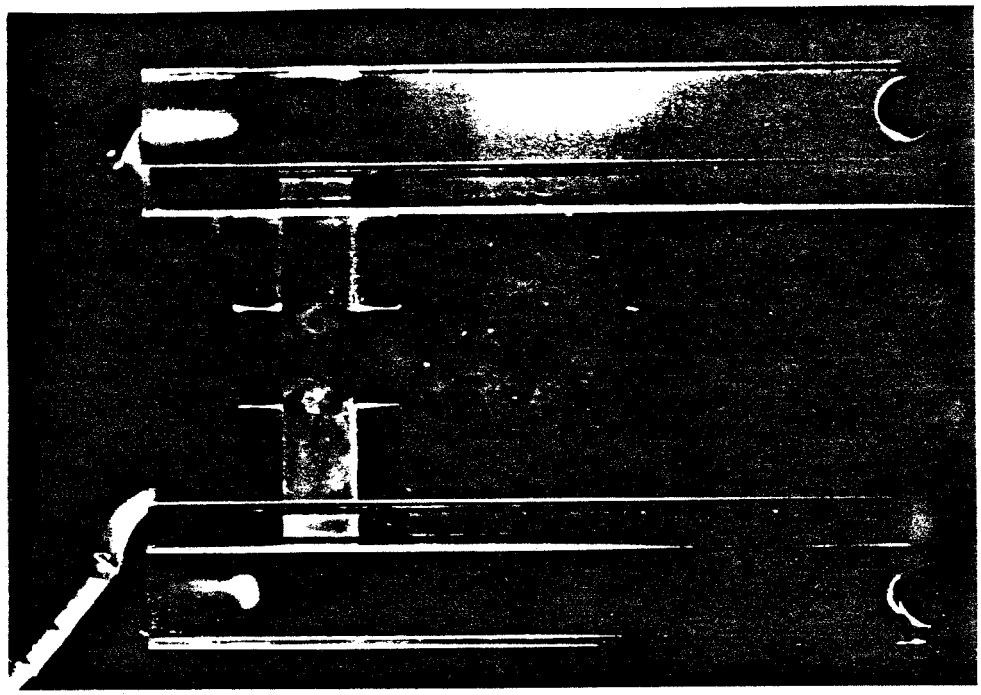

Fig.5.7.1. Flow Visualization for l=1.0 cm and U_e=14 m/sec.

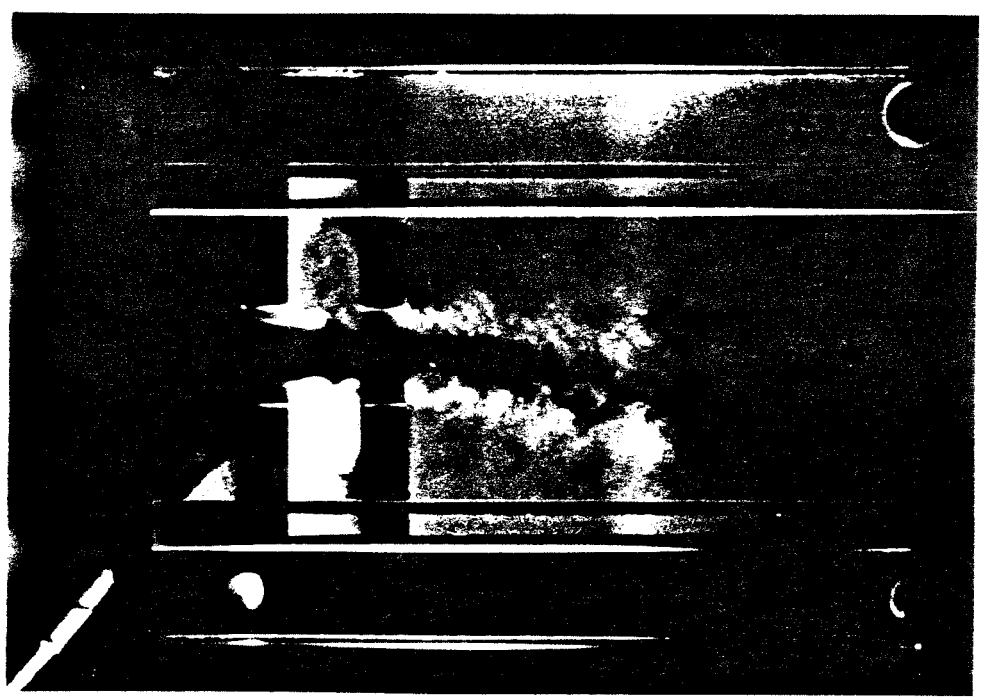

Fig.5.7.2. Flow Visualization for l=1.0 cm and U_e=23 m/sec.

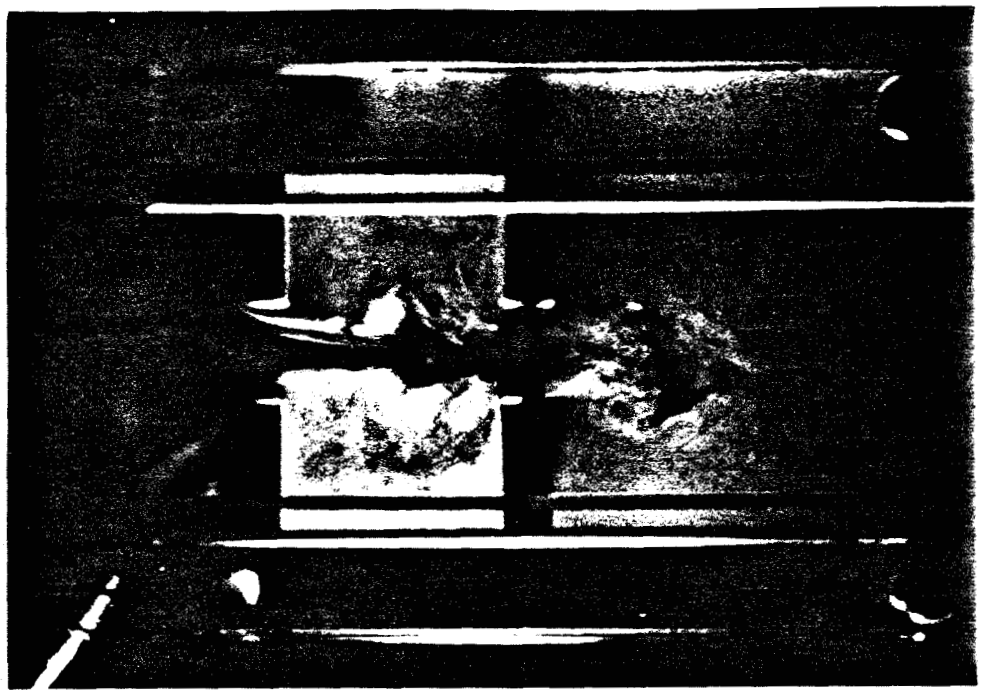

Fig.5.7.3. Flow Visualization for l=3.0 cm and U_e=12 m/sec.

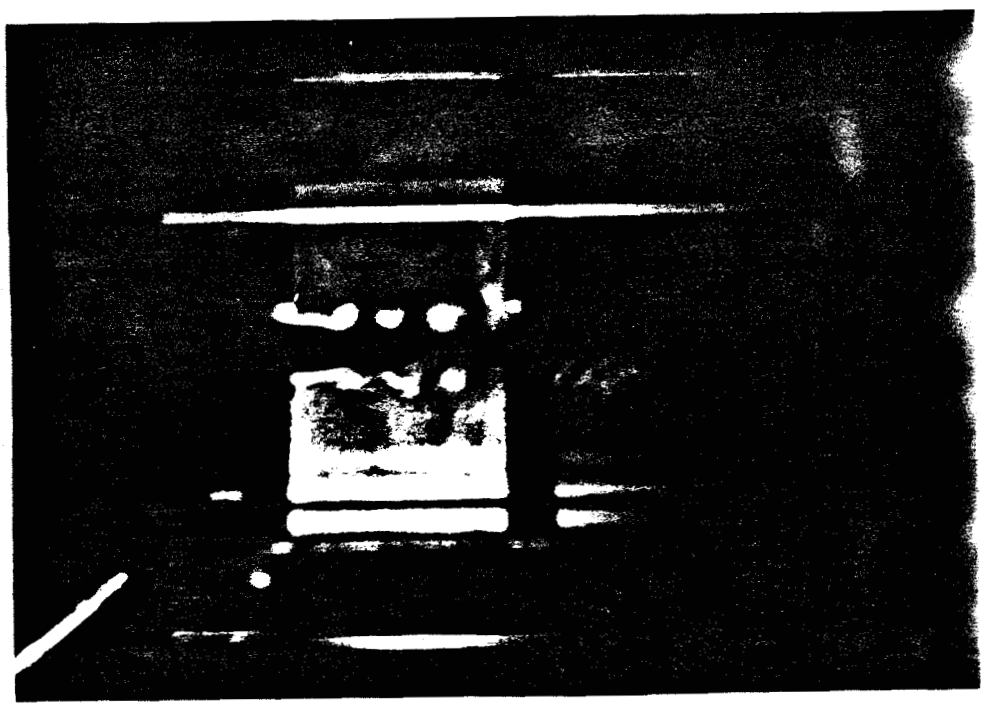

Fig.5.7.4. Flow Visualization for l=3.0 cm and U_e=22 m/sec.

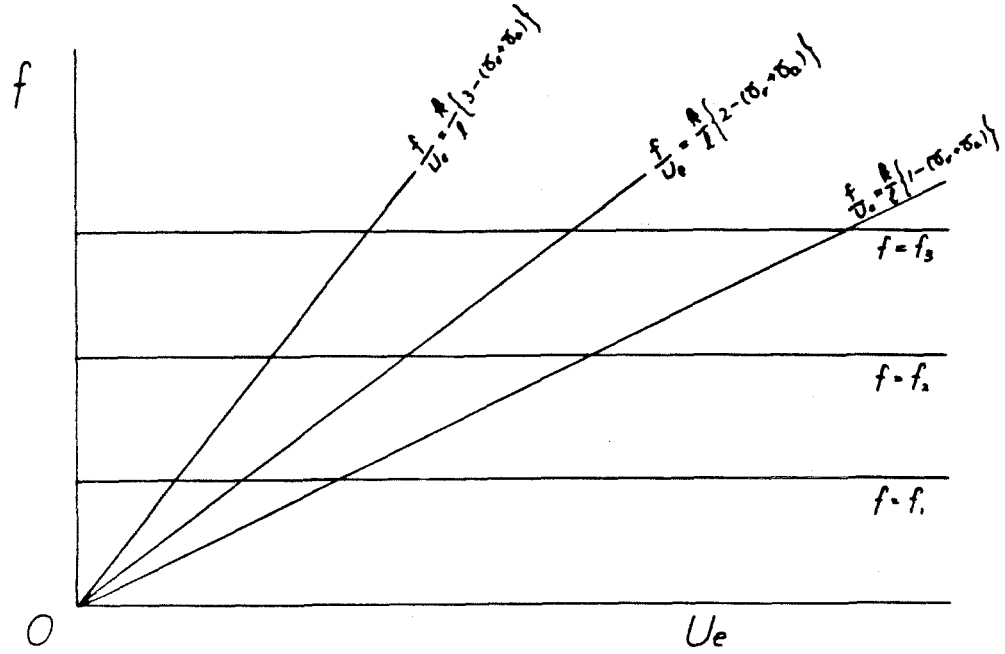

Fig.6.1.1. On the Mechanism of Pure Tone Production.

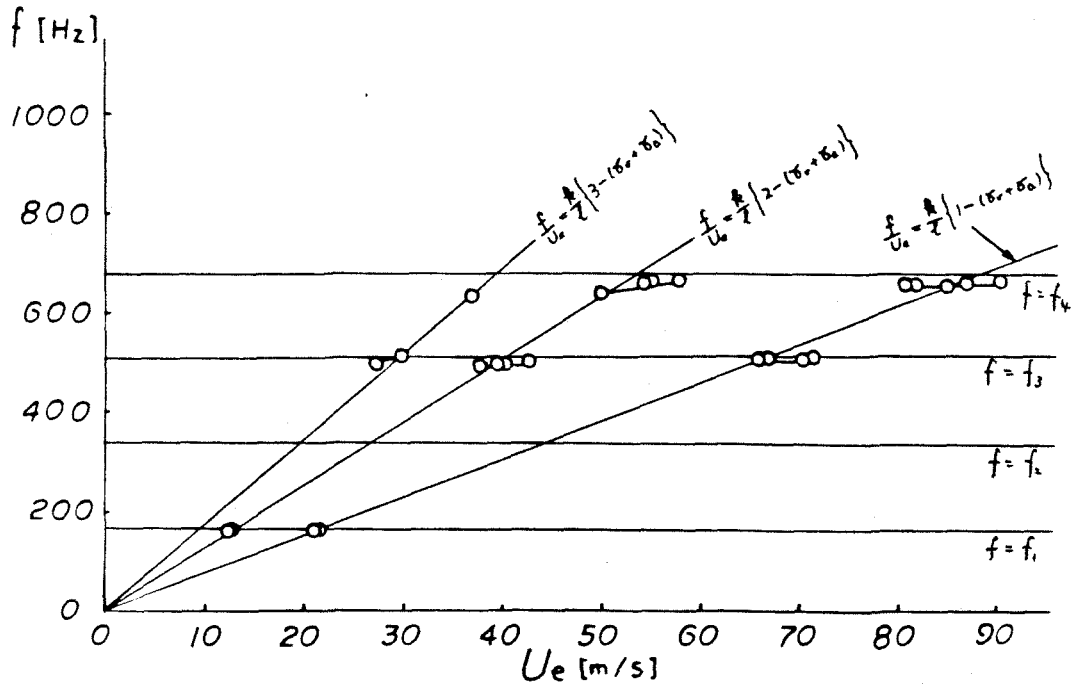

Fig.6.1.2. Pure Tone Frequency.
L=92.7 cm, L_1=20.0 cm, h=1.90 cm and l=3.0 cm.

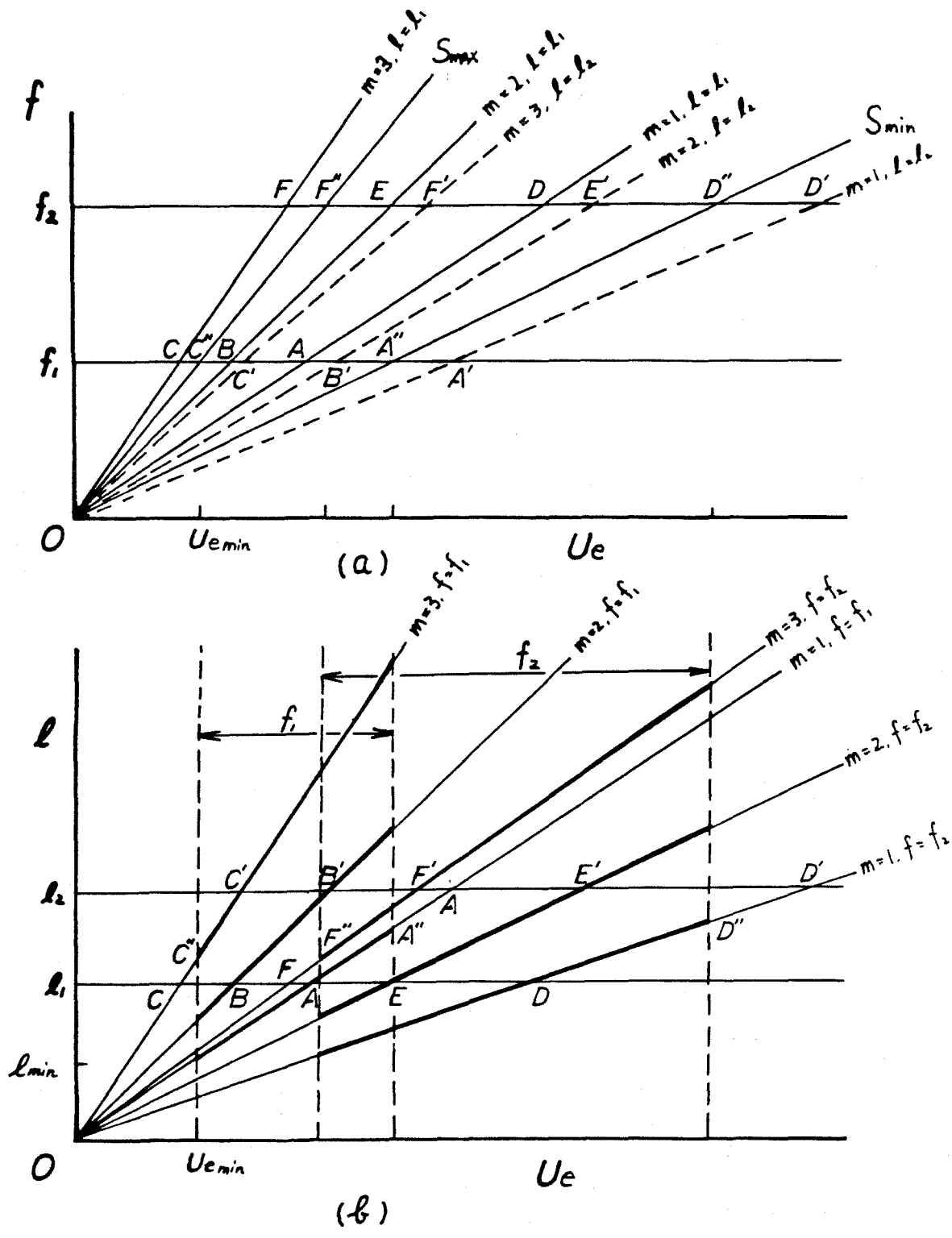

Fig.6.2.1. On the Pure Tone Production Regions.